SIAM J. IMAGING SCIENCES
Vol. 4, No. 2, pp. 501–542

Dual Carrier Probing for Spaceborne SAR Imaging*

E. M. Smith† and S. V. Tsynkov†

Abstract. Spaceborne imaging of the Earth's surface by synthetic aperture radar (SAR) may be adversely affected by the ionosphere that causes distortions of the signals emitted and received by the radar antenna. In our previous publication on the subject [*SIAM J. Imaging Sci.*, 2 (2009) pp. 140–182], we have analyzed those distortions for the inhomogeneous ionosphere described by the cold plasma model. Based on the analysis, we have concluded that the deterioration of SAR images was due to the mismatch between certain parameters of the actual received signal, which is slowed down by the temporal dispersion in the ionosphere, and the corresponding parameters of the matched filter, which is taken as if the propagation were unobstructed. Consequently, to improve the quality of the images, the filter must be corrected. However, to get the appropriate correction, one needs to know some key characteristics of the ionosphere precisely at the time and place the image is taken. To obtain those characteristics, we currently propose probing the terrain, and hence the ionosphere, on two distinct carrier frequencies. We also investigate the performance of the matched filters that were corrected this way and show that the final quality of the images, i.e., their resolution and sharpness evaluated using the SAR ambiguity theory, indeed improves.

Key words. synthetic aperture radar, Earth's ionosphere, dispersion of radio waves, image distortions, cold plasma, matched filter, multicarrier probing, correction of the filter, range and azimuthal resolution, image sharpness

AMS subject classifications. 78A40, 78A45, 78A46, 78A50, 78A55, 78M35, 78M99

DOI. 10.1137/10078325X

1. Introduction.

Synthetic aperture radar (SAR) is a coherent imaging technology which is based predominantly on the phase information of the emitted and received waves (as opposed, say, to conventional photography, which is based on the amplitude). In particular, spaceborne SAR imaging of the Earth's surface involves sending specially shaped pulses of radio waves from the satellite to the ground, receiving the scattered response, and processing it by means of a matched filter [7, 9]. In doing so, the received signal can, in some approximate sense, be interpreted as a Fourier transform of the ground reflectivity function, whereas filtering that yields the image is analogous to the inverse transform. The filter is called matched, because its phase is supposed to match that of the received signal.

When radar signals travel back and forth from the satellite to the surface, they propagate through the Earth's ionosphere and hence undergo temporal dispersion. This causes delays in arrival times. If the filter does not take those delays into account, a mismatch of the phase occurs and, accordingly, the quality of the image deteriorates [41]. The extent of deterioration

*Received by the editors January 20, 2010; accepted for publication (in revised form) March 7, 2011; published electronically May 24, 2011. This work was supported by the US Air Force Office of Scientific Research (AFOSR) under grants FA9550-07-1-0170 and FA9550-10-1-0092.
http://www.siam.org/journals/siims/4-2/78325.html
†Department of Mathematics, North Carolina State University, Box 8205, Raleigh, NC 27695 (emsmith5@ncsu.edu, tsynkov@math.ncsu.edu).

depends on the carrier frequency of the radar, or, more precisely, on its ratio to the Langmuir frequency of the ionospheric plasma. The higher the carrier frequency the less prone the image to ionospheric distortions. Therefore, many modern spaceborne SAR sensors operate in the microwave band on the frequencies of around $10\,GHz$ or even higher. For example, the new European satellite TerraSAR-X operates in the X-band, on the frequencies between $7\,GHz$ and $11.2\,GHz$.

However, there is also substantial interest toward spaceborne SAR technology on lower carrier frequencies, in the VHF or UHF band, i.e., in the range of hundreds of megahertz. Radars of this type have a better surface penetrating capability. On the other hand, their images are much more sensitive to ionospheric distortions. Consequently, special means need to be developed to compensate for those distortions.

In [41], we have analyzed the distortions for the case of SAR imaging by means of a scalar field that propagates through the inhomogeneous ionosphere described by the cold plasma model. We have also proposed probing the terrain, and hence the ionosphere, on two distinct carrier frequencies. This allows one to determine the total electron content (TEC) along the line of sight, which is a key parameter that affects the propagation, and then correct the matched filter accordingly. In the current paper, we investigate the performance of the corrected matched filters. Our main conclusion is that they are capable of completely eliminating the distortions of SAR images due to the deterministic part of the charged particle content in the ionosphere, including the inhomogeneous case. Removing the distortions due to the random part of the charged particle content will be subject of the future work.

To that end, we should point out that the distortions of SAR images, due to the ionospheric randomness (caused by turbulence) can be quantified reasonably well; see, e.g., our previous paper [41], as well as [1, 23, 27, 36]. However, mitigating those distortions requires a substantial additional effort: obtaining the statistics of radio waves based on the statistics of the medium (turbulent ionosphere) (see, e.g., [38, 39, 40]) and then modifying the signal processing algorithm (the matched filter) accordingly. In the literature, this subject has not received too much attention; among the relevant publications we mention [4, 16], where the authors propose several approaches for reducing the random component of the phase error.

We emphasize that the matched filter shall be corrected precisely for the time and place the image is taken. The reason is that the Earth's ionosphere is not steady; its characteristics depend on many factors, such as the time of day, the time of year, geographic location, level of solar activity, etc., and may change rapidly, e.g., considerably faster than the period of one revolution of the satellite around the Earth.

Several approaches to deriving the ionosphere TEC information have been proposed in the literature; some of them are mentioned below, although the review is by no means comprehensive. The authors of [44] rely on the Faraday rotation, which can be used to obtain the TEC in the case of a fully polarimetric quad-channel SAR instrument (see, e.g., [25, section 10.4]). The Faraday rotation is considered the only source of image distortions in [44], and the authors emphasize that for other types of sensors (such as single-channel), an explicit a priori estimate of the Faraday rotation is needed for introducing corrections. The authors of [24] present estimates of the group delays and phase advances for a nonturbulent ionosphere similar to those obtained in our previous paper [41] and again use the Faraday rotation for retrieving the TEC information from the quad-channel SAR data. An earlier publication discussing the effect of

Faraday rotation on polarimetric SAR is [15]. The authors of [30] indicate that in the absence of external information one can use autofocus algorithms (see [14, section 3.9.1] or [12, 43]) to obtain the TEC, which is not a very reliable approach, though, whereas the SAR system itself (L-band) can be efficient in obtaining the difference of the TEC distributions between the two radar acquisitions. The authors of [26] present two approaches: the first one involves a spaceborne radar operating on a very low frequency, below the Langmuir value, and is similar to the traditional ground-based sounding. The second one uses a higher frequency and derives the TEC information by analyzing the returns from the specially chosen bright point targets. The authors of [28] employ a simplified model known as the ionospheric phase screen to analyze the effect of auroral arcs (special electron density irregularities) on spaceborne SAR images taken in the polar regions of the Earth.

Our current paper is organized as follows. In section 2, we describe the physical model and introduce the key assumptions. We note that the conclusions of the paper are valid only if these assumptions are met. In section 3, we build the generalized ambiguity function of a SAR, which provides a key tool for analyzing the radar resolution. In section 4, we discuss the performance of a spaceborne SAR sensor in the case when no attempt is made to mitigate the distortions; this creates a foundation for the subsequent discussion of a corrected matched filter. In section 5, we introduce the dual carrier probing as a venue for obtaining the parameters of the ionosphere (TEC information) needed for correcting the filter. In section 6, we discuss the performance of the radar once the corrected filter has been implemented and show that the resolution and sharpness of the images indeed improve. Finally, section 7 concludes the paper with a summary of what has been accomplished and identifies directions for future work.

We note that in sections 2, 3, and 4 we basically develop a full-fledged radar ambiguity theory for the SAR sensor operating through the Earth's ionosphere (monostatic case). To the best of our knowledge, a mathematical analysis of this type has not been previously reported in the literature, even though there are a number of publications discussing the effects of the ionosphere on SAR imaging; see, e.g., [20] or [45] (a review). An analysis similar to ours is presented in [23] but only for the case of a homogeneous background ionosphere. We refer the reader to our previous paper [41] for a more detailed literature survey.

2. The model.

For the discussion in the current paper we adopt the same model as in [41]. We analyze the standard (as opposed to interferometric) SAR images [14], i.e., all the images are considered two-dimensional (range and azimuth), and the elevation is not taken into account. We also assume that the images are rendered by scalar propagating fields, i.e., that the polarization can be disregarded [7, 9], or, otherwise, that the radar antenna is capable only of transmitting and receiving a single polarization. All the targets are assumed deterministic and dispersionless; scattering of radar signals off the targets is linearized and interpreted using the first Born approximation. The start-stop approximation is employed to describe the synthetic antenna; its applicability to spaceborne SAR sensors (as opposed to airborne) is justified in [42].

The ionosphere is modeled as a layer of inhomogeneous dilute plasma, for which the mean concentration (number density) of electrons depends on the altitude but does not depend on the horizontal coordinates. The latter assumption holds, provided that the characteristic

distances along the Earth's surface are not very large. We disregard the effect of the magnetic field of the Earth on mean electron concentration and assume that the ionosphere is isotropic. This implies, in particular, that the Faraday rotation is not taken into account; of course, for scalar propagating fields (no polarization) it is not considered anyway.

On top of its mean value, the electron number density has a stochastic component due to the ionospheric turbulence, which is a quasi-homogeneous random field [31, 38]. The effect of the Earth's magnetic field on the ionospheric turbulence is disregarded, and the turbulence is assumed isotropic. In the current paper, though, our primary focus will be on the deterministic rather than the stochastic part of the ionospheric phenomena.

The propagation of electromagnetic waves in the ionosphere is analyzed with the help of the cold plasma approximation [17], which requires that the phase speed of the waves be much faster than the thermal speed of the electrons. The cold plasma approximation is equivalent to disregarding spatial dispersion and taking into account only temporal dispersion of radio waves in the plasma [29]. The ionospheric plasma is also assumed lossless; i.e., its Ohm conductivity is disregarded. This means that the effective collision frequencies between different species of particles in the plasma are much lower than the Langmuir frequency. Moreover, the propagation is assumed linear, because the power of signals emitted by spaceborne antennas is typically much lower than that needed for setting off the nonlinear effects; see [18, 21, 22], as well as [17, Chap. VIII].

We use the classical Helmholtz theorem [33] to partition the overall electric field into the longitudinal and transverse components. Then, from the full Maxwell's equations and the equation of motion of electrons in the electric field, one can derive the Klein–Gordon equation (see [41, App. A]) that governs the propagation of high frequency transverse[1] electromagnetic waves in dilute plasma:

$$\frac{\partial^2 \boldsymbol{E}_\perp}{\partial t^2} - c^2 \Delta \boldsymbol{E}_\perp + \omega_{\mathrm{pe}}^2 \boldsymbol{E}_\perp = \boldsymbol{0}. \tag{2.1}$$

The quantity ω_{pe} in (2.1) is the Langmuir frequency, or plasma electron frequency. It characterizes temporal responses of the plasma and is given by

$$\omega_{\mathrm{pe}} = \sqrt{\frac{4\pi e^2 N_{\mathrm{e}}}{m_{\mathrm{e}}}}, \tag{2.2}$$

where e and m_{e} are the charge and mass of the electron, and N_{e} is the electron number density. The behavior of ω_{pe}^2 in the ionosphere follows that of N_{e}; it has an altitude-dependent deterministic component and a stochastic component due to the turbulence. Typical values of the Langmuir frequency in the Earth's ionosphere range between $3MHz$ and $15MHz$.

Unlike in a vacuum, the propagation speed of electromagnetic waves in the ionosphere depends on the frequency. This phenomenon is known as temporal dispersion; it is due to the presence of the last, nondifferentiated, term in (2.1). The dispersion relation for the Klein–Gordon equation reads as

$$\omega^2 = \omega_{\mathrm{pe}}^2 + c^2 k^2. \tag{2.3}$$

[1]The corresponding longitudinal oscillations are known as Langmuir waves; they have zero group velocity [29].

We emphasize that according to (2.3) the short waves are weakly dispersive, whereas the long waves are subject to stronger dispersion. Indeed, the phase and group velocity of the propagation are given by

$$v_{\rm ph} = c\left(1+\omega_{\rm pe}^2/c^2k^2\right)^{\frac{1}{2}} \tag{2.4}$$

and

$$v_{\rm gr} = c\left(1+\omega_{\rm pe}^2/c^2k^2\right)^{-\frac{1}{2}}, \tag{2.5}$$

so that the shorter the wave, (the larger the k) the closer both velocities to the nondispersive limit $v = c$.

In the Cartesian coordinates we can consider (2.1) for individual field components:

$$\frac{\partial^2 E}{\partial t^2} - c^2\Delta E + \omega_{\rm pe}^2 E = 0. \tag{2.6}$$

In the rest of the paper, we will use the scalar governing equation (2.6) to describe the propagation of electromagnetic waves in the ionosphere. For a comprehensive account of the propagation of radio waves in plasma, we refer the reader to the monographs [5, 17].

To characterize the ionospheric turbulence, we write the electron number density as follows:

$$N_{\rm e} = \langle N_{\rm e}\rangle + \mu(\boldsymbol{x}), \tag{2.7}$$

where the angular brackets $\langle\cdot\rangle$ denote the expected value (mean) and μ represents the fluctuations: $\langle\mu\rangle = 0$. In the simplest case of constant $\langle N_{\rm e}\rangle$, $\mu(\boldsymbol{x})$ is a homogeneous and isotropic random field, and its correlation function depends only on the distance $r = |\boldsymbol{x}_1 - \boldsymbol{x}_2|$ and not on the individual locations $\boldsymbol{x}_1$ and $\boldsymbol{x}_2$:

$$V(\boldsymbol{x}_1,\boldsymbol{x}_2) \stackrel{\rm def}{=} \langle\mu(\boldsymbol{x}_1)\mu(\boldsymbol{x}_2)\rangle = V(|\boldsymbol{x}_1-\boldsymbol{x}_2|) \equiv V(r). \tag{2.8}$$

In reality, however, $\langle N_{\rm e}\rangle$ is a function of the altitude h. At the same time, the ratio

$$M = \frac{\sqrt{\langle\mu^2\rangle}}{\langle N_{\rm e}\rangle} \tag{2.9}$$

is assumed altitude independent. A typical numerical value of M is $5\cdot 10^{-3}$, and in extreme situations it may reach 10^{-1} [1]. Hence, $\sqrt{\langle\mu^2\rangle}$ also depends on h, which makes $\mu(\boldsymbol{x})$ a quasi-homogeneous (rather than truly homogeneous) random field. While in this case we still keep the same notation (2.8) for the correlation function, in fact we have $V = V(h,r)$, where the dependence on h (altitude) is slow and the dependence on r (local variable) is fast. Hereafter, we will use the exponential correlation function

$$V(r) = C\pi^2 q_0^3 e^{-q_0 r}. \tag{2.10}$$

It accounts only for the short range phenomena in the ionosphere and has the spectrum [32, sect. 12.1]

$$\widehat{V}(q) = \frac{C}{(1+q^2/q_0^2)^\kappa}, \quad \text{where} \quad \kappa = 2 \ \text{ and } \ C = \text{const}. \tag{2.11}$$

In formulae (2.10) and (2.11), we denote $q_0 = r_0^{-1}$, where r_0 is the correlation length or outer scale of turbulence. The latter may range between $1km$ and $10km$ according to different sources in the literature. An advantage of using the correlation function (2.10) is that one can easily make sure that it satisfies a necessary and sufficient condition of ergodicity given in [31, sect. 4.7] (a 1938 theorem by E. E. Slutskii):

$$\lim_{S\to\infty} \frac{1}{S} \int_0^S V(s)ds = 0. \tag{2.12}$$

Ergodicity implies that statistical means can be substituted for spatial averages of μ whenever averaging is done over sufficiently long intervals. In that regard we note that if a random field is ergodic, then it must have $\langle\mu\rangle = \text{const}$, because the spatial average of μ does not depend on the location, whereas its statistical mean $\langle\mu\rangle$ may, generally speaking, be a function of the coordinates [31, sect. 4.6]. In our particular case, however, we have $\langle\mu\rangle = 0$, which means that ergodicity can be employed even when the random field μ is quasi-homogeneous rather than truly homogeneous (because its variance depends on the altitude).

It should also be mentioned that for the true Kolmogorov-type turbulence we have $\kappa = 11/6$ rather than $\kappa = 2$ in formula (2.11); see [38, Chap. I]. From the standpoint of practice, the difference between the two cases is that $\kappa = 11/6$ allows one to take into account some long range phenomena in the ionosphere. As we have indicated in [41], this is a separate interesting subject for future study.

For the purpose of obtaining specific quantitative estimates, we will use the same typical values of the parameters as we have exploited in [41]. A reference value of the mean electron concentration will be taken as $\langle N_\text{e}\rangle = 10^6 cm^{-3}$ (in fact, $\langle N_\text{e}\rangle = \langle N_\text{e}(h)\rangle$), which corresponds to the F-layer of the ionosphere and yields $\omega_\text{pe} \approx 9MHz$. The radar carrier frequency will be assumed equal to $1GHz$, which is the lower bound for the microwave band and yields the wavelength $\lambda = 30cm$. According to [3], it is very difficult to achieve high resolution of spaceborne SAR images for carrier frequencies under $1GHz$ if no attempt is made to reduce the distortions due to the ionosphere. A typical one-way propagation distance between the satellite and the ground will be taken as $R_0 \approx 1000km$, and the orbit altitude H may be about $500km$ or higher. Other important parameters will be introduced as needed.

3. The generalized ambiguity function. The generalized ambiguity function offers a convenient way of assessing the radar performance. It is basically the image of a point target, i.e., that of a delta-type scatterer. In the ideal world, this image would be a delta-function as well. In reality, however, it is smeared out (by the nature of the radar signal processing, even when there is no ionosphere and no dispersion), and the extent of this smearing provides the limits of radar resolution.

The interrogating pulses emitted by the antenna of a SAR are taken as linear upchirps[2] of the form

$$P(t) = A(t)e^{i\omega_0 t}, \quad \text{where} \quad A(t) = \chi_\tau(t)e^{i\alpha t^2}. \tag{3.1}$$

In formula (3.1), $\chi_\tau(t)$ is the indicator function of the interval of duration τ:

$$\chi_\tau(t) = \begin{cases} 1, & t \in [-\tau/2, \tau/2], \\ 0 & \text{otherwise}, \end{cases}$$

and $\alpha = B/(2\tau)$, where B is the bandwidth of the chirp. Accordingly, the instantaneous frequency of the chirp [7, 9] is given by

$$\omega(t) = \omega_0 + \frac{Bt}{\tau}, \quad t \in [-\tau/2, \tau/2], \tag{3.2}$$

where ω_0 is the center carrier frequency. The modulating function $A(t)$ in formula (3.1) is assumed slowly varying compared to the fast carrier oscillation $e^{i\omega_0 t}$. A typical duration of the pulse in actual SAR systems may be $\tau \sim 5 \cdot 10^{-5} sec$, a typical interval between two consecutive pulses may be $\sim 5 \cdot 10^{-4} sec$, and the bandwidth in formula (3.2) is $B \sim 10 MHz$ (it may be higher).

Hereafter, the radar is assumed to operate in the stripmap mode (see [6]), when the antenna points in a fixed direction relative to that of the satellite motion.[3] Hence, the footprint of the beam emitted by the antenna sweeps a strip on the Earth's surface parallel to the flight track, i.e., to the orbit.

To obtain the image, the antenna emits a series of pulses (3.1) when moving along the orbit. Those pulses travel to the Earth's surface, get scattered off the ground, and propagate back toward the satellite, where they are received by the same antenna (in the case of a monostatic SAR [6]). In doing so, clearly, both the emission and the reception of pulses are done by a moving antenna (which gives rise to the Doppler frequency shift), and, moreover, the satellite travels a certain distance along the orbit during the pulse round-trip time between the antenna and the ground. However, in a simplified framework of the start-stop approximation, those effects are disregarded. Instead, we assume that the pulse is emitted and the scattered response received while the antenna is at a standstill at one and the same position, after which it moves to its next sending/receiving position along the orbit. This assumption has been used extensively in the SAR literature, as it renders the corresponding analysis much easier. It, however, needs to be justified, especially when the antenna moves fast, such as when it is mounted on a satellite as opposed to an airplane. A full justification for the use of start-stop approximation for spaceborne SAR imaging can be found in [42].

3.1. Nondispersive propagation. We first derive the generalized ambiguity function for the case of unobstructed propagation with the speed c. In this case, the field is governed by the standard d'Alembert equation, which is obtained from the Klein–Gordon equation (2.6)

[2] These are high-range resolution waveforms; see [9].

[3] When this direction is normal to the flight track, the imaging is referred to as broadside.

by dropping the last term, i.e., by setting $\omega_{\rm pe} = 0$. As indicated in section 2, all images are assumed two-dimensional with range and azimuth (i.e., cross-range) being the coordinates, and the elevation of the target above the Earth's surface is not taken into account. This applies to the analysis of both nondispersive and dispersive cases.

Suppose that the antenna is a motionless point source located at $\boldsymbol{x} \in \mathbb{R}^3$. Then the propagating field due to the emitted chirp (3.1) is given by the standard retarded potential of the d'Alembert operator:

$$\varphi(t,\boldsymbol{z}) = \frac{1}{4\pi}\frac{P(t-|\boldsymbol{z}-\boldsymbol{x}|/c)}{|\boldsymbol{z}-\boldsymbol{x}|}. \tag{3.3}$$

Let us assume that the imaged terrain, which is also motionless, is characterized by the variable refraction index $n = n(\boldsymbol{z})$. Under the first Born approximation [2, sect. 13.1.4], scattering is linearized so that the terrain is interpreted as a secondary wave's source due to the incident field $\varphi(t,\boldsymbol{z})$ of (3.3):

$$\frac{1-n^2(\boldsymbol{z})}{c^2}\frac{\partial^2\varphi}{\partial t^2} \stackrel{\rm def}{=} \nu(\boldsymbol{z})\frac{\partial^2\varphi}{\partial t^2}.$$

Consequently, the scattered field at the location $\boldsymbol{x}$ of the antenna and the moment of time t is given by the Kirchhoff integral:

$$\psi(t,\boldsymbol{x}) = \frac{1}{4\pi}\iiint_{|\boldsymbol{x}-\boldsymbol{z}|\le ct}\frac{\nu(\boldsymbol{z})}{|\boldsymbol{x}-\boldsymbol{z}|}\frac{\partial^2\varphi}{\partial t^2}\,(t-|\boldsymbol{x}-\boldsymbol{z}|/c,\boldsymbol{z})\,d\boldsymbol{z}. \tag{3.4}$$

As the amplitude $A(t)$ in (3.1) is slowly varying, it can be left out when differentiating the incident field (3.3) for substitution into (3.4), which yields

$$\frac{\partial^2\varphi}{\partial t^2}(t,\boldsymbol{z}) \approx -\frac{\omega_0^2}{4\pi}\frac{P(t-|\boldsymbol{z}-\boldsymbol{x}|/c)}{|\boldsymbol{z}-\boldsymbol{x}|}. \tag{3.5}$$

Consequently,

$$\begin{aligned}\psi(t,\boldsymbol{x}) &\approx -\frac{\omega_0^2}{16\pi^2}\iiint_{|\boldsymbol{x}-\boldsymbol{z}|\le ct}\frac{\nu(\boldsymbol{z})}{|\boldsymbol{x}-\boldsymbol{z}|^2}P\,(t-2|\boldsymbol{x}-\boldsymbol{z}|/c)\,d\boldsymbol{z}\\ &= -\frac{\omega_0^2}{16\pi^2}\iiint_{|\boldsymbol{x}-\boldsymbol{z}|\le ct}\frac{\nu(\boldsymbol{z})}{|\boldsymbol{x}-\boldsymbol{z}|^2}A\,(t-2|\boldsymbol{x}-\boldsymbol{z}|/c)\,e^{i\omega_0(t-2|\boldsymbol{x}-\boldsymbol{z}|/c)}d\boldsymbol{z}.\end{aligned} \tag{3.6}$$

According to (3.6), the scattered field $\psi(t,\boldsymbol{x})$ can be interpreted a result of application of a Fourier integral operator (FIO) to the ground reflectivity function $\nu(\boldsymbol{z})$; see, e.g., [8, 9, 10, 34].The FIO is approximately inverted by applying a matched filter to ψ and accumulating the information due to multiple interrogating pulses (3.1) emitted from and received by the antenna at different locations on the orbit. This procedure is similar to application of the adjoint operator, which would have coincided with the true inverse if the mapping (3.6) were a standard Fourier transform.

The matched filter is defined as follows. Assume that there is a point scatterer at the reference location $\boldsymbol{y}$; then the resulting field at $(t, \boldsymbol{x})$ is obtained by substituting $\nu(\boldsymbol{z}) = \delta(\boldsymbol{z} - \boldsymbol{y})$ into formula (3.6):

$$\psi_1(t, \boldsymbol{x}) = -\frac{\omega_0^2}{16\pi^2} \frac{P(t - 2|\boldsymbol{x} - \boldsymbol{y}|/c)}{|\boldsymbol{x} - \boldsymbol{y}|^2}. \tag{3.7}$$

The filter is essentially a complex conjugate of ψ_1 given by (3.7); for simplicity, the constant factor $-\omega_0^2/16\pi^2$, as well the entire denominator, which is a slowly varying function (compared to the fast oscillation $e^{i\omega_0 t}$), are disregarded. What remains is merely $\overline{P(t - 2|\boldsymbol{x} - \boldsymbol{y}|/c)}$, where the overbar denotes complex conjugation. The idea of building the filter this way, i.e., the idea of matching, is to have the large phase cancel in the exponent; see formula (3.1). The application of this filter yields a single-look image:

$$\begin{aligned} I(\boldsymbol{y}) &= \int \overline{P(t - 2|\boldsymbol{x} - \boldsymbol{y}|/c)} \psi(t, \boldsymbol{x}) dt \\ &= -\frac{\omega_0^2}{16\pi^2} \iiint_{|\boldsymbol{x}-\boldsymbol{z}| \le ct} \underbrace{\int \overline{P(t - 2|\boldsymbol{x} - \boldsymbol{y}|/c)} P(t - 2|\boldsymbol{x} - \boldsymbol{z}|/c) dt}_{W(\boldsymbol{y}, \boldsymbol{z})} \frac{\nu(\boldsymbol{z})}{|\boldsymbol{x} - \boldsymbol{z}|^2} d\boldsymbol{z}, \end{aligned} \tag{3.8}$$

where we have changed the order of integration after substituting expression (3.6) for $\psi(t, \boldsymbol{x})$. The interior integral $W(\boldsymbol{y}, \boldsymbol{z})$ in formula (3.8) is called the point spread function; see [7, 9]. Up to a slowly varying denominator, the point spread function $W(\boldsymbol{y}, \boldsymbol{z})$ yields a single-look image of the point scatterer located at $\boldsymbol{z}$; i.e., it is the field due to a unit magnitude delta-function at $\boldsymbol{z}$ processed with the matched filter $\overline{P(\,\cdot\,)}$.

As, however, has been mentioned, the full SAR image is built using multiple looks, when the antenna emits a sequence of chirps (3.1) from different locations on the orbit. It is precisely this approach based on incorporating the information from multiple looks that enables drastic improvements in the quality of the image compared to the single look strategy [7, 9]. Let us therefore consider a sequence of emitting/receiving times and locations $(t_n, \boldsymbol{x}^n)$. For each n, we build the point spread function following (3.8):

$$W_n(\boldsymbol{y}, \boldsymbol{z}) = \int \overline{P(t - t_n - 2|\boldsymbol{x}^n - \boldsymbol{y}|/c)} P(t - t_n - 2|\boldsymbol{x}^n - \boldsymbol{z}|/c) dt. \tag{3.9}$$

The generalized ambiguity function of a SAR system takes into account the information from multiple interrogating pulses by summing up the corresponding contributions (3.9):

$$W(\boldsymbol{y}, \boldsymbol{z}) = \sum_n \vartheta(\boldsymbol{z}, \boldsymbol{x}^n) W_n(\boldsymbol{y}, \boldsymbol{z}). \tag{3.10}$$

The factor $\vartheta(\boldsymbol{z}, \boldsymbol{x}^n)$ under the sum in (3.10) determines the range of summation. It comes from the directivity pattern of the antenna, because the actual SAR antenna is never a point monopole. The quantity $\vartheta(\boldsymbol{z}, \boldsymbol{x}^n)$ can be approximated as follows:

$$\vartheta(\boldsymbol{z}, \boldsymbol{x}^n) = \begin{cases} 1 & \text{if the target } \boldsymbol{z} \text{ is in the beam emitted from } \boldsymbol{x}^n, \\ 0 & \text{otherwise.} \end{cases}$$

In [41, App. B] (see also [7, 9]) we have shown that the antenna of longitudinal dimension L emits a beam of angular width $2\lambda/L$, provided that the carrier wavelength $\lambda = 2\pi c/\omega_0$ is much shorter than L. Consequently, the longitudinal size of the antenna footprint on the ground in the case of broadside imaging is

$$R_0 \tan\frac{\lambda}{L} \approx R_0\frac{\lambda}{L},$$

where R_0 is the distance from the location of the antenna $\boldsymbol{x}^n$ to the center of the footprint. Therefore,

$$\vartheta(\boldsymbol{z},\boldsymbol{x}^n) = \begin{cases} 1 & \text{if } z_1 - R_0\frac{\lambda}{L} \le x_1^n \le z_1 + R_0\frac{\lambda}{L}, \\ 0 & \text{if } x_1^n < z_1 - R_0\frac{\lambda}{L} \text{ or } x_1^n > z_1 + R_0\frac{\lambda}{L}, \end{cases} \tag{3.11}$$

where the subscript "1" denotes the coordinate direction along the flight track (orbit).

The range of summation in (3.10) is therefore defined by taking into account only those $\boldsymbol{x}^n$ for which $\vartheta(\boldsymbol{z},\boldsymbol{x}^n) = 1$; see (3.11). Let Δx_1 be the distance along the orbit between the successive emissions of pulses. We can also take $z_1 = 0$ with no loss of generality. Then the inequality $-\frac{\lambda R_0}{L} \le x_1^n \le \frac{\lambda R_0}{L}$ translates into $-\frac{N}{2} \le n \le \frac{N}{2}$, where $N = [\frac{2\lambda R_0}{\Delta x_1 L}]$ and $[\,\cdot\,]$ is the integer part. Consequently, we recast (3.9), (3.10) as

$$\begin{aligned} W(\boldsymbol{y},\boldsymbol{z}) = \sum_{-N/2}^{N/2} \int & \overline{A(t - t_n - 2|\boldsymbol{y}-\boldsymbol{x}^n|/c)} e^{2i\omega_0|\boldsymbol{y}-\boldsymbol{x}^n|/c} \\ & \times A(t - t_n - 2|\boldsymbol{z}-\boldsymbol{x}^n|/c) e^{-2i\omega_0|\boldsymbol{z}-\boldsymbol{x}^n|/c} dt. \end{aligned} \tag{3.12}$$

Next, we change the integration variable from t to $t - t_n$ in each term of the sum (3.12) and realize that neither $\overline{A(t - 2|\boldsymbol{y}-\boldsymbol{x}^n|/c)}$ nor $A(t - 2|\boldsymbol{z}-\boldsymbol{x}^n|/c)$ depends on n explicitly, except for the dependence via $\boldsymbol{x}^n$. The latter is weak, because for large R_0 both $|\boldsymbol{y}-\boldsymbol{x}^n|$ and $|\boldsymbol{z}-\boldsymbol{x}^n|$ are slowly varying functions of $\boldsymbol{x}^n$, and they appear as arguments of another slowly varying function, A. Hence, the factors $\bar{A}$ and A can be taken out of the sum (3.12), and $\boldsymbol{x}^n$ inside $\overline{A(\,\cdot\,)}$ and $A(\,\cdot\,)$ can be replaced by $\boldsymbol{x}^0$ for definiteness, which yields

$$W(\boldsymbol{y},\boldsymbol{z}) \approx \Bigg(\underbrace{\int \overline{A(t - 2|\boldsymbol{y}-\boldsymbol{x}^0|/c)} A(t - 2|\boldsymbol{z}-\boldsymbol{x}^0|/c) dt}_{W_R(\boldsymbol{y},\boldsymbol{z})} \Bigg) \Bigg(\underbrace{\sum_{-N/2}^{N/2} e^{2i\omega_0(|\boldsymbol{y}-\boldsymbol{x}^n|/c - |\boldsymbol{z}-\boldsymbol{x}^n|/c)}}_{W_A(\boldsymbol{y},\boldsymbol{z})} \Bigg). \tag{3.13}$$

Hence, the generalized ambiguity function gets approximately split into the product of the range factor

$$W_R(\boldsymbol{y},\boldsymbol{z}) = \int \overline{A(t - 2|\boldsymbol{y}-\boldsymbol{x}^0|/c)} A(t - 2|\boldsymbol{z}-\boldsymbol{x}^0|/c) dt \tag{3.14}$$

and the azimuthal factor

$$W_A(\boldsymbol{y},\boldsymbol{z}) = \sum_{n=-N/2}^{N/2} e^{2i\omega_0(|\boldsymbol{y}-\boldsymbol{x}^n|/c-|\boldsymbol{z}-\boldsymbol{x}^n|/c)} \tag{3.15}$$

that control the range and azimuthal resolution of the radar,[4] respectively (see [7, 9]), in the case of unobstructed propagation between the orbit and the ground. Indeed, the generalized ambiguity function (3.13) is the image of a delta-type scatterer. Hence, if we could make it equal to a delta-function as well, $W(\boldsymbol{y},\boldsymbol{z}) = \delta(\boldsymbol{y}-\boldsymbol{z})$, then the radar would have had perfect resolution. In reality this is never achieved, and instead $W(\boldsymbol{y},\boldsymbol{z})$ has a peak of finite height and finite width when the reference point $\boldsymbol{y}$ approaches the target $\boldsymbol{z}$. The sharper (i.e., the narrower) this peak the better the resolution, because two sharper peaks can be told apart if they are closer.

3.2. Dispersive propagation in the homogeneous medium. In the case of propagation through the ionosphere, both the shape and the speed of the pulse change, because of the dispersion. The simplest case to analyze is that of a homogeneous ionosphere; a detailed analysis (based on the Fourier transform and linearization) is provided in Appendix A. The form of the propagating pulse emitted by the antenna at $\boldsymbol{x}$ is given by (A.16) (cf. formula (3.3)):

$$\varphi(t,\boldsymbol{z}) = \frac{A'(t-|\boldsymbol{z}-\boldsymbol{x}|/v_{\rm gr}(\omega_0))}{4\pi|\boldsymbol{z}-\boldsymbol{x}|} e^{i\omega_0(t-|\boldsymbol{z}-\boldsymbol{x}|/v_{\rm ph}(\omega_0))}, \quad \text{where} \quad A'(t) = \chi_{\tau'}(t)e^{i\alpha' t^2}, \tag{3.16}$$

and τ' and α' are the new chirp duration and rate given by (A.12) and (A.15), respectively:

$$\tau' = \tau + \delta\tau = \tau + 2\frac{|\boldsymbol{z}-\boldsymbol{x}|}{c}\frac{\omega_{\rm pe}^2}{\omega_0^2}\frac{B}{\omega_0} \tag{3.17}$$

and

$$\alpha' = \alpha + \delta\alpha = \alpha - \frac{|\boldsymbol{z}-\boldsymbol{x}|}{c}\frac{\omega_{\rm pe}^2}{\omega_0^3}\frac{B^2}{\tau^2} = \alpha - \frac{\delta\tau}{2}\frac{B}{\tau^2} = \frac{B}{2\tau}\left(1-\frac{\delta\tau}{\tau}\right). \tag{3.18}$$

Let us emphasize that unlike in a vacuum, the shape of the pulse keeps changing as it propagates through the plasma; according to (3.17) and (3.18), the longer the distance $|\boldsymbol{z}-\boldsymbol{x}|$ that the pulse travels, the more it gets dilated (τ' becomes longer) and the more its rate decreases (α' becomes smaller).

[4] Resolution is a capability of the radar to distinguish between two different targets located a certain distance apart.

We also emphasize that as formula (3.16) indicates, the chirp itself, i.e., its slowly varying envelope A', which presents a physical observable, travels with the group velocity $v_{\rm gr}(\omega_0)$ that corresponds to the center carrier frequency ω_0. For the high frequency case that we are interested in, $\omega_0 \gg \omega_{\rm pe}$, the group velocity (2.5) can be linearized:

$$v_{\rm gr} = v_{\rm gr}(\omega) \approx c\left(1 - \frac{1}{2}\frac{\omega_{\rm pe}^2}{c^2k^2}\right) = c\left(1 - \frac{1}{2}\frac{\omega_{\rm pe}^2}{\omega^2 - \omega_{\rm pe}^2}\right) \approx c\left(1 - \frac{1}{2}\frac{\omega_{\rm pe}^2}{\omega^2}\right). \tag{3.19}$$

At the same time, the center carrier oscillation per se, i.e., the wave $e^{i\omega_0 t}$, travels with the corresponding phase velocity $v_{\rm ph}(\omega_0)$ that can also be linearized:

$$v_{\rm ph} = v_{\rm ph}(\omega) \approx c\left(1 + \frac{1}{2}\frac{\omega_{\rm pe}^2}{c^2k^2}\right) = c\left(1 + \frac{1}{2}\frac{\omega_{\rm pe}^2}{\omega^2 - \omega_{\rm pe}^2}\right) \approx c\left(1 + \frac{1}{2}\frac{\omega_{\rm pe}^2}{\omega^2}\right). \tag{3.20}$$

Using the notions of the group and phase velocities (3.19) and (3.20), we can introduce the group and phase travel times, respectively, in the homogeneous ionosphere,

$$T_{\rm gr}(\boldsymbol{x},\boldsymbol{z},\omega) = \frac{|\boldsymbol{x}-\boldsymbol{z}|}{v_{\rm gr}(\omega)} \quad \text{and} \quad T_{\rm ph}(\boldsymbol{x},\boldsymbol{z},\omega) = \frac{|\boldsymbol{x}-\boldsymbol{z}|}{v_{\rm ph}(\omega)}, \tag{3.21}$$

and recast formula (3.16) as follows:

$$\varphi(t,\boldsymbol{z}) = \frac{A'(t - T_{\rm gr}(\boldsymbol{x},\boldsymbol{z},\omega_0))}{4\pi|\boldsymbol{z}-\boldsymbol{x}|} e^{i\omega_0(t - T_{\rm ph}(\boldsymbol{x},\boldsymbol{z},\omega_0))}. \tag{3.22}$$

It is important to point out that the group velocity $v_{\rm gr}$ of (3.19) is slower than the speed of light c, as it is supposed to be for any velocity associated with the propagation of physical observables. However, the phase velocity $v_{\rm ph}$ (3.20) is faster than the speed of light c. Hence, if we introduce the neutral (nondispersive) travel time $T = T(\boldsymbol{x},\boldsymbol{z}) = |\boldsymbol{x}-\boldsymbol{z}|/c$, then, according to (3.19) and (3.20), for the group and phase travel times we can write

$$\begin{gathered} T_{\rm gr}(\boldsymbol{x},\boldsymbol{z},\omega) = T(\boldsymbol{x},\boldsymbol{z}) + \Delta T \quad \text{and} \quad T_{\rm ph}(\boldsymbol{x},\boldsymbol{z},\omega) = T(\boldsymbol{x},\boldsymbol{z}) - \Delta T, \\ \text{where} \quad \Delta T = \Delta T(\boldsymbol{x},\boldsymbol{z},\omega) = \frac{|\boldsymbol{x}-\boldsymbol{z}|}{c}\frac{1}{2}\frac{\omega_{\rm pe}^2}{\omega^2}. \end{gathered} \tag{3.23}$$

In other words, the group delay and the phase advance in formula (3.22) are equal to one another. Given (3.23), we can recast formula (3.17) for the pulse dilation as follows:

$$\delta\tau = 4\Delta T(\boldsymbol{x},\boldsymbol{z},\omega_0)\frac{B}{\omega_0}. \tag{3.24}$$

It shall also be noted that in the previous paper [41], we used a simpler semiqualitative approach to analyze the propagation of chirps in the ionosphere. The result was the same as (3.22) with one important difference, though: Instead of the phase advance that characterizes the propagation of the carrier frequency in formula (3.22), in [41] we have incorporated a phase delay equal to the group delay. This could not affect the analysis of the range resolution, as

it is based on the propagation of envelopes; see formula (3.14). On the other hand, this could potentially affect our analysis of the azimuthal resolution in [41], as the azimuthal factor of the generalized ambiguity function (3.15) includes the phase information. However, as shown by subsequent analysis in the current paper, our previous calculations of the azimuthal resolution are not affected either, because in the linearized high frequency framework that we employ, the group delay and the phase advance are equal in magnitude; see formulae (3.23).

3.3. Dispersive propagation in the inhomogeneous medium. In the actual ionosphere, the electron number density N_{e} is not constant, and this is going to affect the propagation times (3.21). For the analysis in this paper, we will assume that the mean electron number density $\langle N_{\mathrm{e}}\rangle$ depends on the altitude above the Earth's surface but does not depend on the horizontal coordinates. A typical dependence of the mean electron number density on the altitude h is nonmonotonic. The maximum is reached in the F-layer somewhere between $200km$ and $300km$ above the Earth's surface, and the characteristic scale h_0 of the variations of $\langle N_{\mathrm{e}}\rangle$ is on the order of tens of kilometers; see [17, Chap. VI]. Clearly, $h_0 \gg \lambda$, where λ is the wavelength, which suggests that we can perhaps use the approximation of geometrical optics to analyze the propagation of SAR pulses in the inhomogeneous ionosphere.

We should remember, however, that the total electron number density N_{e} also has a stochastic component $\mu(\boldsymbol{x})$; see formula (2.7). It depends on all spatial coordinates and can be interpreted as a quasi-homogeneous random field. To justify the use of geometrical optics for the study of pulse propagation through the turbulent ionosphere, the wavelength λ must be much shorter than the characteristic scale of turbulent inhomogeneities. If the latter is taken as r_0 (the outer scale of turbulence), the constraint $\lambda \ll r_0$ is obviously met. There is, however, a more subtle criterion for applicability of the geometrical optics. The characteristic scale of inhomogeneities must be much longer than the size of the first Fresnel zone $\sqrt{\lambda R_{\boldsymbol{z}}}$, where $R_{\boldsymbol{z}} = |\boldsymbol{z} - \boldsymbol{x}|$ is the propagation distance between the antenna and the target. The quantity $\sqrt{\lambda R_{\boldsymbol{z}}}$ comes to approximately $540m$ for $\lambda = 30cm$ and $R_{\boldsymbol{z}} = 1000km$, which is roughly $\frac{1}{2}r_0$ according to [1] or $\frac{1}{20}r_0$ according to [4]. Technically speaking, this makes the geometrical optics a borderline approximation for the class of problems we are considering. It is known, however, that there are fewer shorter scale inhomogeneities in the spectrum of ionospheric turbulence than longer scale inhomogeneities, which still leaves the main conclusions of geometrical optics valid even outside its formal applicability range; see [39, Chap. I].

The expressions for travel times in the inhomogeneous ionosphere that replace formulae (3.21) are derived in Appendix B for the deterministic case and in Appendix C for the stochastic case. The final expressions that we present correspond to the stochastic formulae (C.15) and (C.16); they reduce to the deterministic formulae (B.21) and (B.22) if $\mu = 0$:

$$T_{\mathrm{gr}}(\boldsymbol{x},\boldsymbol{z},\omega) = \frac{R_{\boldsymbol{z}}}{c}\left[1 + \frac{1}{2}\frac{4\pi e^2}{m_{\mathrm{e}}\omega^2}\left(\frac{\bar{N}_{\mathrm{e}}^{(H)}}{H} + \frac{1}{R_{\boldsymbol{z}}}\int_0^{R_{\boldsymbol{z}}} \mu(s)ds\right)\right], \tag{3.25a}$$

$$T_{\mathrm{ph}}(\boldsymbol{x},\boldsymbol{z},\omega) = \frac{R_{\boldsymbol{z}}}{c}\left[1 - \frac{1}{2}\frac{4\pi e^2}{m_{\mathrm{e}}\omega^2}\left(\frac{\bar{N}_{\mathrm{e}}^{(H)}}{H} + \frac{1}{R_{\boldsymbol{z}}}\int_0^{R_{\boldsymbol{z}}} \mu(s)ds\right)\right]. \tag{3.25b}$$

The quantity $\bar{N}_{\mathrm{e}}^{(H)}$ in formulae (3.25) is defined by (C.8), and H denotes the orbit altitude.

Similarly to (3.23), we can also write

(3.26)
$$T_{\rm gr}(\boldsymbol{x},\boldsymbol{z},\omega)=T(\boldsymbol{x},\boldsymbol{z})+\Delta T\quad\text{and}\quad T_{\rm ph}(\boldsymbol{x},\boldsymbol{z},\omega)=T(\boldsymbol{x},\boldsymbol{z})-\Delta T,$$

$$\text{where}\quad T(\boldsymbol{x},\boldsymbol{z})=\frac{R_z}{c}\quad\text{and}\ \Delta T=\Delta T(\boldsymbol{x},\boldsymbol{z},\omega)=\frac{R_z}{c}\frac{1}{2}\frac{4\pi e^2}{m_{\rm e}\omega^2}\Bigg(\underbrace{\frac{\bar N_{\rm e}^{(H)}}{H}+\frac{1}{R_z}\int_0^{R_z}\mu(s)ds}_{\mathcal{N}}\Bigg).$$

Given the travel times (3.26), we can evaluate the dilation of the pulse on its way between the antenna $\boldsymbol{x}$ and the target $\boldsymbol{z}$ using formula (3.24):

$$\delta\tau=4\Delta T(\boldsymbol{x},\boldsymbol{z},\omega_0)\frac{B}{\omega_0}=\frac{2R_z}{c}\frac{4\pi e^2}{m_{\rm e}\omega_0^2}\frac{B}{\omega_0}\mathcal{N}. \tag{3.27}$$

On the way between the antenna and the target and back, the dilation (3.27) doubles, because the travel distance doubles. The pulse rate (3.18) changes accordingly.

Finally, we can modify the generalized ambiguity function derived in section 3.1 (see formula (3.13)) by substituting the actual travel times (3.25) instead of the unobstructed travel time $|\boldsymbol{z}-\boldsymbol{x}^0|/c$ into those factors that correspond to the received signal. According to the form (3.22) of the propagating pulse, the group travel time $T_{\rm gr}(\boldsymbol{x}^0,\boldsymbol{z},\omega_0)$ of (3.25a) shall be substituted into $W_R(\boldsymbol{y},\boldsymbol{z})$ and the phase travel time $T_{\rm ph}(\boldsymbol{x}^n,\boldsymbol{z},\omega_0)$ of (3.25b) shall be substituted into $W_A(\boldsymbol{y},\boldsymbol{z})$. Then, instead of formulae (3.14) and (3.15), we have

$$W_R'(\boldsymbol{y},\boldsymbol{z})=\int\overline{A(t-2|\boldsymbol{y}-\boldsymbol{x}^0|/c)}A_{2\delta\tau}'(t-2T_{\rm gr}(\boldsymbol{x}^0,\boldsymbol{z},\omega_0))dt \tag{3.28}$$

and

$$W_A'(\boldsymbol{y},\boldsymbol{z})=\sum_{n=-N/2}^{N/2}e^{2i\omega_0(|\boldsymbol{y}-\boldsymbol{x}^n|/c-T_{\rm ph}(\boldsymbol{x}^n,\boldsymbol{z},\omega_0))}. \tag{3.29}$$

The subscript $2\delta\tau$ in formula (3.28) indicates that the round-trip pulse dilation is twice the $\delta\tau$ of (3.27).

We emphasize that in formulae (3.28) and (3.29) the factors that correspond to the actual field received by the antenna take into account the dispersion of radio waves in the ionosphere. However, the factors that represent the matched filter remain the same as in the nondispersive case. This creates a mismatch, and as has been shown in [41], it is precisely this mismatch that is responsible for the deterioration of the image. In the next section, we briefly reproduce the corresponding arguments from [41]. It will also help us better understand the mechanism of correcting the matched filter proposed in this paper.

4. Performance of the radar with noncorrected filter.

4.1. Range resolution. Integration (3.28) has been performed in [41, App. C]. Up to a factor of magnitude one, integral (3.28) takes the form

$$W_R'(\boldsymbol{y},\boldsymbol{z})\propto\int_{\max\{-\tau/2+2R_y/c,\,-\tau'/2+2T_{\rm gr}(\boldsymbol{x}^0,\boldsymbol{z},\omega_0)\}}^{\min\{\tau/2+2R_y/c,\,\tau'/2+2T_{\rm gr}(\boldsymbol{x}^0,\boldsymbol{z},\omega_0)\}}e^{i(\alpha'-\alpha)t^2}e^{4i(\alpha R_y/c-\alpha' T_{\rm gr}(\boldsymbol{x}^0,\boldsymbol{z},\omega_0))t}dt, \tag{4.1}$$

where $R_{\boldsymbol{y}} = |\boldsymbol{y} - \boldsymbol{x}^0|$. In the simplest case, we disregard the quadratic term in the exponent under the integral (4.1). Then, taking the limits as $\mp\tau/2+2R_{\boldsymbol{y}}/c$ and changing the integration variable $t = u + 2R_{\boldsymbol{y}}/c$, we have

$$W'_R(\boldsymbol{y}, \boldsymbol{z}) \propto \tau \operatorname{sinc}\left(2[\alpha' R_{\boldsymbol{y}}/c - \alpha' T_{\mathrm{gr}}(\boldsymbol{x}^0, \boldsymbol{z}, \omega_0)]\tau\right). \tag{4.2}$$

When analyzing radar resolution, the $\operatorname{sinc} x \stackrel{\mathrm{def}}{=} \frac{\sin x}{x}$ function is what one typically gets instead of the "genuine" δ-function; see [7, 9]. The sharper the central peak of the sinc (i.e., its main lobe between the first zeros on either side of the maximum), the "closer" it is to the δ-function and hence the better the resolution. The width (or, sometimes, semiwidth) of the main lobe of the sinc is actually taken as a measure of radar resolution, because it is considered the distance at which two such peaks can be clearly told apart.

In the nondispersive case, $T(\boldsymbol{x}^0, \boldsymbol{z}, \omega_0) = R_{\boldsymbol{z}}/c$ and $\alpha' = \alpha$. Hence, $W'_R(\boldsymbol{y}, \boldsymbol{z})$ reduces to $W_R(\boldsymbol{y}, \boldsymbol{z})$ and, consequently, the sinc attains its maximum when $R_{\boldsymbol{y}} = R_{\boldsymbol{z}}$, i.e., when the distance from the antenna to the reference location $\boldsymbol{y}$ coincides with that for the target location $\boldsymbol{z}$. The resolution is then controlled by how widely the sinc is "spread around" its central maximum. The semiwidth of the main lobe of the sinc corresponds to the value of its argument equal to π, and therefore for the full width we find $\Delta R = 2\pi c/B$. It is the quantity ΔR that is interpreted as the range resolution, i.e., the minimum distance, at which the SAR system can distinguish between two point targets located on the same line of sight normal to the orbit.

The situation with the dispersive range factor $W'_R(\boldsymbol{y}, \boldsymbol{z})$ of (4.2) is somewhat different. The maximum of the sinc is attained when its full argument is zero, i.e., when $R_{\boldsymbol{y}} = cT(\boldsymbol{x}^0, \boldsymbol{z}, \omega_0)$, which yields

$$R_{\boldsymbol{y}} - R_{\boldsymbol{z}} = cT(\boldsymbol{x}^0, \boldsymbol{z}, \omega_0) - R_{\boldsymbol{z}} = R_{\boldsymbol{z}} \frac{1}{\omega_0^2} \frac{4\pi e^2}{2m_{\mathrm{e}}} \mathcal{N}. \tag{4.3}$$

This is obviously not equivalent to $R_{\boldsymbol{y}} - R_{\boldsymbol{z}} = 0$, which implies that on the image the target is shifted in range from its absolute position by the value of the right-hand side of (4.3). The range resolution per se, however, is still given by the width of the main lobe of the sinc as a function of the argument $R_{\boldsymbol{y}} - R_{\boldsymbol{z}}$:

$$\Delta R = \frac{\pi c}{\alpha' \tau} = \frac{2\pi c}{B}\left(1 + \frac{2\delta\tau}{\tau}\right). \tag{4.4}$$

The factor of 2 in front of $\delta\tau$ in (4.4) appears, because the pulse dilation is evaluated for the round trip between the antenna and the target. The relative deterioration of the range resolution compared to the nondispersive case is therefore $\sim 2\delta\tau/\tau$; see (4.4). As shown in [41], for the typical values of all the relevant parameters in the deterministic ionosphere, this quantity is very small, about 0.02%.

If the quadratic term is retained in the exponent under the integral (4.1) after the change of variables, then the integration yields a complex-valued function $W'_R(\boldsymbol{y}, \boldsymbol{z})$ rather than the actual sinc. As shown in [41], the maxima and minima of its absolute value $|W'_R(\boldsymbol{y}, \boldsymbol{z})|$ are located precisely where the maxima and zeros of the sinc are. In this sense, the range resolution

remains unchanged. However, instead of the actual zeros the new $|W_R'(\boldsymbol{y},\boldsymbol{z})|$ now has minima with some nonzero values. In particular, for the first minimum we have

$$|W_R'(\boldsymbol{y},\boldsymbol{z})|\Big|_{4\alpha'(R_y/c-T(\boldsymbol{x}^0,\boldsymbol{z},\omega_0))=\frac{2\pi}{\tau}} = \tau\frac{\delta\alpha\tau^2}{\pi^2}\left(1+\mathcal{O}(\delta\alpha\tau^2)\right). \tag{4.5}$$

The right-hand side of equality (4.5) is about $0.02\cdot\tau$ for the typical parameters involved. Therefore, the dispersion of radio waves in the ionosphere causes a deterioration of the image sharpness. As the central maximum of $|W_R'(\boldsymbol{y},\boldsymbol{z})|$ basically remains equal to τ, the extent of deterioration appears to be 2%, but this value can, of course, vary both ways depending on the parameters of the radar and the conditions of the ionosphere.

Let us also recall that the quantity $\mathcal{N}$ that determines the dilation of the pulse and its new rate (see formulae (3.27) and (3.18)), as well as the shift of the target position (see formula (4.3)), does not only contain a deterministic component but also a stochastic one. The latter is the average value of μ along the ray trajectory; see (3.25). Hence, based on the idea of ergodicity, and recalling that $\langle\mu\rangle = 0$, we can expect that the effect of the aforementioned stochastic component on the radar performance in range will not be large.

To quantify this argument further, we denote the random contribution to $T_{\rm gr}(\boldsymbol{x}^0,\boldsymbol{z},\omega)$ by

$$\varphi_0 = \int_0^{R_z}\mu(s)ds, \quad R_{\boldsymbol{z}} = |\boldsymbol{x}^0-\boldsymbol{z}|, \quad \langle\varphi_0\rangle = 0, \tag{4.6}$$

where the integration is conducted along the unperturbed trajectory, and also introduce the mean dilation according to (3.27):

$$\langle\delta\tau\rangle = \frac{2R_{\boldsymbol{z}}}{c}\frac{4\pi e^2}{m_{\rm e}\omega_0^2}\frac{B}{\omega_0}\langle\mathcal{N}\rangle = \frac{2R_{\boldsymbol{z}}}{c}\frac{4\pi e^2}{m_{\rm e}\omega_0^2}\frac{B}{\omega_0}\frac{\bar{N}_{\rm e}^{(H)}}{H}.$$

Standard deviations of both φ_0 and $\delta\tau$ were computed in [41] using the spectrum of turbulent fluctuations (2.11). It was also shown that $\sqrt{\langle\varphi_0^2\rangle} \ll \bar{N}_{\rm e}^{(H)}$ and $\sqrt{\langle\delta\tau^2\rangle} \ll \langle\delta\tau\rangle$, or, more precisely, for the case of a homogeneous ionosphere,

$$\frac{\sqrt{\langle\varphi_0^2\rangle}}{\bar{N}_{\rm e}^{(H)}} = \frac{\sqrt{\langle\delta\tau^2\rangle}}{\langle\delta\tau\rangle} \approx \sqrt{\frac{r_0}{R_{\boldsymbol{z}}}}M \ll 1,$$

where r_0 is the correlation length, and M is given by (2.9). In the case of a stratified ionosphere, the variance of fluctuations becomes a function of the altitude h: $\langle\mu^2\rangle = \langle\mu^2(h)\rangle$, and one can show [41] that

$$\sqrt{\frac{\langle\varphi_0^2\rangle}{\bar{N}_{\rm e}^{2,(H)}\cdot H}} \approx \sqrt{\frac{r_0}{R_{\boldsymbol{z}}}}M, \quad \text{where} \quad \bar{N}_{\rm e}^{2,(H)} = \int_0^H \langle N_{\rm e}(h)\rangle^2 dh. \tag{4.7}$$

According to [1], the value of $\bar{N}_{\rm e}^{2,(H)}$ for high altitudes H is between $9.3\cdot10^{18}cm^{-5}$ and $9.9\cdot10^{20}cm^{-5}$, with the average about $1.5\cdot10^{19}cm^{-5}$. Then, say, for $H = 500km$ we have $(\bar{N}_{\rm e}^{2,(H)}\cdot H)^{1/2} \approx 2.7\cdot10^{13}cm^{-2}$, which is close to $\bar{N}_{\rm e}^{(H)} \sim \langle N_{\rm e}\rangle\cdot H \approx 5\cdot10^{13}cm^{-2}$ if one takes $\langle N_{\rm e}\rangle =$

$10^6 cm^{-3}$. We therefore conclude that the contribution of turbulent fluctuations to travel delays, as well as to the change of the pulse shape during its propagation in the ionosphere, is much smaller than that of the baseline dispersion. Therefore, the role of randomness in the deterioration of SAR performance in range appears minute and can be disregarded for the typical values of the parameters involved.

4.2. Azimuthal resolution. The azimuthal factor (3.29) of the generalized ambiguity function has also been computed in [41]. Similarly to (4.6), let us denote

$$\varphi_n = \int_0^{R_z} \mu(s)ds, \quad R_{\boldsymbol{z}} = |\boldsymbol{x}^n - \boldsymbol{z}|. \tag{4.8}$$

We also linearize the travel distances:

$$\begin{aligned} R_{\boldsymbol{z}} &= |\boldsymbol{z} - \boldsymbol{x}^n| = \sqrt{R_0^2 + (z_1 - x_1^n)^2} = R_0\sqrt{1 + \frac{(x_1^n)^2}{R_0^2}} \approx R_0\left(1 + \frac{1}{2}\frac{(x_1^n)^2}{R_0^2}\right), \\ R_{\boldsymbol{y}} &= |\boldsymbol{y} - \boldsymbol{x}^n| = \sqrt{R_0^2 + (y_1 - x_1^n)^2} = R_0\sqrt{1 + \frac{(y_1 - x_1^n)^2}{R_0^2}} \approx R_0\left(1 + \frac{1}{2}\frac{(y_1 - x_1^n)^2}{R_0^2}\right), \end{aligned} \tag{4.9}$$

because $|x_1^n| \ll R_0$ and $|y_1 - x_1^n| \ll R_0$, where R_0 is the distance along the normal (recall that the subscript "1" denotes the coordinate along the orbit, and $z_1 = 0$, as in section 3.1). Then, up to a factor of magnitude one, formula (3.29) along with (3.25b) yields

$$W_A'(\boldsymbol{y}, \boldsymbol{z}) \propto \sum_{n=-N/2}^{N/2} e^{\frac{2i\omega_0}{c}\left(-\frac{y_1 x_1^n}{R_0} + \frac{1}{2}\frac{(x_1^n)^2}{2R_0}\frac{4\pi e^2}{m_e\omega_0^2}\frac{\bar{N}_e^{(H)}}{H} + \frac{1}{2}\frac{4\pi e^2}{m_e\omega_0^2}\varphi_n\right)}. \tag{4.10}$$

According to the central limit theorem, for long integration distances $R_{\boldsymbol{z}}$ each quantity φ_n of (4.8) becomes a Gaussian random variable with zero mean; see [39, Chap. I]. Hence, the mean of each term of (4.10) is

$$\begin{aligned} &\left\langle e^{\frac{2i\omega_0}{c}\left(-\frac{y_1 x_1^n}{R_0} + \frac{1}{2}\frac{(x_1^n)^2}{2R_0}\frac{4\pi e^2}{m_e\omega_0^2}\frac{\bar{N}_e^{(H)}}{H} + \frac{1}{2}\frac{4\pi e^2}{m_e\omega_0^2}\varphi_n\right)}\right\rangle \\ &= e^{\frac{2i\omega_0}{c}\left(-\frac{y_1 x_1^n}{R_0} + \frac{1}{2}\frac{(x_1^n)^2}{2R_0}\frac{4\pi e^2}{m_e\omega_0^2}\frac{\bar{N}_e^{(H)}}{H}\right)}\frac{1}{\sqrt{2\pi\langle\varphi_n^2\rangle}}\int_{-\infty}^{\infty} e^{\frac{i\omega_0}{c}\frac{4\pi e^2}{m_e\omega_0^2}\xi} e^{-\frac{\xi^2}{2\langle\varphi_n^2\rangle}} d\xi \\ &= e^{\frac{2i\omega_0}{c}\left(-\frac{y_1 x_1^n}{R_0} + \frac{1}{2}\frac{(x_1^n)^2}{2R_0}\frac{4\pi e^2}{m_e\omega_0^2}\frac{\bar{N}_e^{(H)}}{H}\right)} e^{-\frac{1}{2}\frac{\omega_0^2}{c^2}\left(\frac{4\pi e^2}{m_e\omega_0^2}\right)^2\langle\varphi_n^2\rangle}, \end{aligned} \tag{4.11}$$

and the variance is given by (see [41])

$$\sigma_n^2 = e^{-\frac{\omega_0^2}{c^2}\left(\frac{4\pi e^2}{m_e\omega_0^2}\right)^2\langle\varphi_n^2\rangle}\left(e^{\frac{\omega_0^2}{c^2}\left(\frac{4\pi e^2}{m_e\omega_0^2}\right)^2\langle\varphi_n^2\rangle} - 1\right) \approx \frac{\omega_0^2}{c^2}\left(\frac{4\pi e^2}{m_e\omega_0^2}\right)^2\langle\varphi_n^2\rangle. \tag{4.12}$$

The (dimensionless) quantity on the right-hand side of (4.12), which is obtained by Taylor's formula, is the variance of the phase; it is small for the typical values of the parameters

involved. Thus, the decrease of the amplitude on the right-hand side of (4.11) is also small; in the literature it is known as extinction [39, Chap. I].

To obtain the mean and variance of the sum (4.10), we will assume that all individual variances (4.12) are the same: $\sigma_n^2 = \sigma^2$, $n = -N/2, \ldots, N/2$. To that effect we note that while the integration distance $R_{\boldsymbol{z}}$ in formula (4.8) depends on n, its variation compared to R_0 is small; see (4.9).

For the mean value of (4.10) we can therefore write using (4.11)

$$\langle W_A'(\boldsymbol{y},\boldsymbol{z})\rangle \;\propto\; e^{-\sigma^2/2}\sum_{n=-N/2}^{N/2} e^{\frac{2i\omega_0}{c}\left(-\frac{y_1 x_1^n}{R_0}+\frac{1}{2}\frac{(x_1^n)^2}{2R_0}\frac{4\pi e^2}{m_e\omega_0^2}\frac{\bar{N}_e^{(H)}}{H}\right)}, \tag{4.13}$$

where the deterministic sum on the right-hand side of (4.13) controls the azimuthal resolution in the case of a nonfluctuating ionosphere. There are two terms in the exponent on the right-hand side of (4.13). The first one, linear with respect to x_1^n, is the only thing that one would have obtained if the propagation were unobstructed. The second term, which is quadratic with respect to x_1^n, is due to the phase mismatch between the actual received signal subject to ionospheric delays and the noncorrected matched filter.

With no quadratic term we have

$$\sum_{n=-N/2}^{N/2} e^{-\frac{2i\omega_0}{c}\frac{y_1 x_1^n}{R_0}} \approx (N+1)\mathrm{sinc}\frac{\omega_0 y_1 \Delta x_1 (N+1)}{R_0 c}, \tag{4.14}$$

where Δx_1 is the distance that the satellite travels along the orbit between the successive emission of pulses, $x_1^n = n\cdot\Delta x_1$, and we have assumed that $\frac{\omega_0 y_1 \Delta x_1}{R_0 c} \ll 1$, which holds for the typical values of all parameters. The semiwidth of the main lobe of the sinc corresponds to the value of its argument equal to π:

$$\frac{2\pi y_1 \Delta x_1}{R_0\lambda}\frac{2\lambda R_0}{\Delta x_1 L} = \pi,$$

where we have replaced $N+1$ by $N = [\frac{2\lambda R_0}{\Delta x_1 L}] \approx \frac{2\lambda R_0}{\Delta x_1 L}$, because $N \gg 1$ ($\Delta x_1 \approx 4m$ for the satellite travel speed of $8km/sec$). Consequently, the azimuthal resolution in the undistorted case is $2y_1 = L/2$.

With the quadratic term taken into account, the function $\langle W_A'(\boldsymbol{y},\boldsymbol{z})\rangle$ of (4.13) becomes complex valued. The central maximum of its modulus is attained when the argument is equal to zero, and the first minimum appears precisely where the first zero of the sinc (4.14) is. In this sense, the azimuthal resolution per se remains unaffected. However, similarly to the case of range resolution, the sharpness of the image deteriorates, and this deterioration for the azimuthal resolution appears stronger. Specifically, one can show [41] that

$$|\langle W_A'(\boldsymbol{y},\boldsymbol{z})\rangle|\Big|_{\frac{\omega_0 y_1 \Delta x_1 (N+1)}{R_0 c}=\pi} \approx e^{-\sigma^2/2}\,(N+1)\frac{\omega_0(\Delta x_1)^2}{2R_0 c}\frac{4\pi e^2}{m_e\omega_0^2}\frac{\bar{N}_e^{(H)}}{H}\frac{(N+1)^2}{2\pi^2}, \tag{4.15}$$

which is approximately $0.09\cdot(N+1)$ for the typical values of the parameters involved. Hence, there may be about 9% degradation of image sharpness in the azimuthal direction due to the dispersion of radio waves in the ionosphere.

The effect of randomness on the azimuthal resolution is also stronger than that on the range resolution. Recall that range resolution is basically determined by a single look, and because of the ergodicity the contribution of turbulent fluctuations into the radar reading on this single look effectively vanishes (i.e., averages out). On the contrary, azimuthal resolution is determined based on multiple looks, $n = -N/2, \dots, N/2$, and whereas the contribution of randomness into each individual reading is still small, it can get amplified when those individual readings are summed up. In [41], we call this effect "unaveraging."

To estimate the variance of the sum (4.10), one needs to see to what extent the individual random variables that compose this sum are dependent or independent. Each of these random variables has a logarithmically normal probability distribution, and similarly to the standard Gaussian variables, if they are uncorrelated, they are independent [41, App. F]. Therefore, the covariance (correlation function) of the received field along the synthetic antenna can provide a measure of dependence or independence for the random variables that compose the sum (4.10). In [39, Chap. I] it is shown that if the fluctuations of the phase are small, then the correlation function for the field approximately coincides with the correlation function for the electron number density (2.8). Consequently, the correlation length r_0 (see formula (2.11)) will also provide a characteristic scale of how rapidly the received field decorrelates along the synthetic antenna. Roughly speaking, for the locations that are further apart than r_0, the received pulses will be uncorrelated and hence independent, whereas for the locations that are closer than r_0 they will not be independent.

Based on these considerations, the following expression was obtained in [41] for the variance of (4.10):

$$\sigma_\Sigma^2 = \frac{D}{r_0} N_c^2 \sigma^2 = \frac{r_0}{D}(N+1)^2\sigma^2, \tag{4.16}$$

where $D = R_0 \frac{2\lambda}{L}$ is the length of the synthetic array. It has also been shown in [41] that the corresponding relative change of the azimuthal resolution is $\frac{\sigma}{2}\sqrt{\frac{r_0}{D}}$. This quantity is about 0.3% for the typical values of the parameters, and it is also proportional to $\omega_0^{-1/2}$, i.e., increases as the carrier frequency decreases.

A 0.3% degradation of the azimuthal resolution is not negligible but is still rather small. However, when estimating σ via $\langle\varphi^2\rangle$ (see formulae (4.7) and (4.12)), we have taken the average values for M and $N_{\mathrm{e}}^{2,(H)}$. Taking the corresponding values from the upper part of their respective ranges may result in a much larger value of $\langle\varphi^2\rangle$ and, as such, in a noticeable deterioration of azimuthal resolution.

5. Dual carrier probing. To remove the mismatch that causes distortions of the image, one needs to correct the filter, i.e., replace the unobstructed travel times $|\boldsymbol{y} - \boldsymbol{x}^n|/c$ by $T_{\mathrm{gr}}(\boldsymbol{x}^n, \boldsymbol{y}, \omega_0)$ in (3.28) and by $T_{\mathrm{ph}}(\boldsymbol{x}^n, \boldsymbol{y}, \omega_0)$ in (3.29), and also adjust the chirp duration and chirp rate in the filter factor under the integral (3.28). However, unlike in the received field, which is a physical observable, the correction in the filter must be done theoretically. Therefore, one needs to know the quantity $\mathcal{N}$ (see formula (3.26)) that characterizes the ionosphere. The availability of $\mathcal{N}$ will allow one to calculate the dilation (3.27) and the new chirp rate (3.18) for any reference location $\boldsymbol{y}$.

The quantity $\mathcal{N}$ depends on the deterministic part of the electron number density (see formula (C.8)) and also has a random component obtained by integrating $\mu(\boldsymbol{x})$ along the ray trajectory. In the literature, many estimates are available for the electron number density and the TEC in the ionosphere; see, e.g., [17] or [5]. Those estimates, however, can provide only a typical range of values, especially as the parameters of the ionosphere are known to vary in space and in time. This will not allow one to correct the filter with a sufficient degree of reliability. More accurate values of the ionospheric parameters can be obtained with the help of the specialized techniques, such as those described in the papers surveyed in section 1. It is to be emphasized, though, that even if the TEC is known accurately, but not for the exact same state of the ionosphere that corresponds to having a given image taken, it may still be not very useful for mitigating the image distortions. What is needed rather is an accurate value of $\mathcal{N}$ exactly at the time and place the image is taken. The technique we describe hereafter provides just that.

Namely, we exploit the idea of dual carrier probing as it applies to deriving $\mathcal{N}$ for the given specific state of the ionosphere. Let us assume that there is an object or feature in the scene that can be clearly identified on the image. This object does not have to be artificial. It does not have to dominate the scene, say, by having the highest reflectivity. Its location does not have to be known ahead of time. It merely has to be something that can be fairly easily picked out and matched on different images that represent the same terrain. For example, it can be some landmark, such as a hilltop, a building, a road intersection, etc.

Let ω_0 and ω_1 be two distinct carrier frequencies, $\omega_0 \neq \omega_1$, and let $R_{\boldsymbol{y}}^{(0)}$ and $R_{\boldsymbol{y}}^{(1)}$ be the corresponding ranges of the aforementioned object measured by the radar, whereas its true range is $R_{\boldsymbol{z}}$ (unknown yet). Then we can consider the corresponding two equations (4.3) as a system:

$$\begin{aligned} R_{\boldsymbol{y}}^{(0)} &= cT_{\mathrm{gr}}(\boldsymbol{x}^0, \boldsymbol{z}, \omega_0), \\ R_{\boldsymbol{y}}^{(1)} &= cT_{\mathrm{gr}}(\boldsymbol{x}^0, \boldsymbol{z}, \omega_1), \end{aligned} \tag{5.1}$$

where the group travel time T_{gr} is given by formula (3.25a). With the data $R_{\boldsymbol{y}}^{(0)}$ and $R_{\boldsymbol{y}}^{(1)}$ available, system (5.1) can be solved with respect to the two unknown quantities: the true range $R_{\boldsymbol{z}}$ and the integral quantity $\mathcal{N}$ that characterizes the plasma.

More precisely, the true range $R_{\boldsymbol{z}}$ enters into the expression for T_{gr} as a factor in front of the formula and also as the integration limit for the random component of the electron number density; see (3.25a). As, however, we have seen in section 4, the contribution of randomness into the single-look image is very small for large $R_{\boldsymbol{z}}$, because of the ergodicity. Randomness rather manifests itself when the information from multiple looks is combined for the analysis of azimuthal resolution. Therefore, since system (5.1) contains only single-look information, we can disregard the stochastic contribution into T_{gr} and instead of (3.25a) substitute the expression

$$\tilde{T}_{\mathrm{gr}}(\boldsymbol{x}^0, \boldsymbol{z}, \omega) = \frac{R_{\boldsymbol{z}}}{c}\left[1 + \frac{1}{\omega^2}\frac{4\pi e^2}{2m_{\mathrm{e}}}\frac{\bar{N}_{\mathrm{e}}^{(H)}}{H}\right] \tag{5.2}$$

on the right-hand side of equations (5.1). We emphasize that the simplification offered by formula (5.2) compared to formula (3.25a) is due to the ergodicity of μ that can be employed

in the context of single-look imaging. This simplification is important, as it allows one to determine the plasma quantity $\bar{N}_{\mathrm{e}}^{(H)}$ defined by formula (C.8), as well as the true range $R_{\boldsymbol{z}}$.

Let us introduce the following notation for brevity:

$$\bar{\omega}_{\mathrm{pe}}^2 = \frac{4\pi e^2}{m_{\mathrm{e}}} \frac{\bar{N}_{\mathrm{e}}^{(H)}}{H}. \tag{5.3}$$

Using this notation, system (5.1) with the expression for $\tilde{T}_{\mathrm{gr}}$ given by (5.2) is recast as

$$\begin{aligned} R_{\boldsymbol{y}}^{(0)} &= R_{\boldsymbol{z}} \left(1 + \frac{\bar{\omega}_{\mathrm{pe}}^2}{2\omega_0^2} \right), \\ R_{\boldsymbol{y}}^{(1)} &= R_{\boldsymbol{z}} \left(1 + \frac{\bar{\omega}_{\mathrm{pe}}^2}{2\omega_1^2} \right). \end{aligned} \tag{5.4}$$

The range $R_{\boldsymbol{z}}$ can be eliminated from system (5.4) by dividing the equations by one another. Then, after simple transformations, we have

$$\bar{\omega}_{\mathrm{pe}}^2 = \frac{2\omega_0^2\omega_1^2(R_{\boldsymbol{y}}^{(0)} - R_{\boldsymbol{y}}^{(1)})}{\omega_1^2 R_{\boldsymbol{y}}^{(1)} - \omega_0^2 R_{\boldsymbol{y}}^{(0)}}. \tag{5.5}$$

Once the frequency $\bar{\omega}_{\mathrm{pe}}^2$ has been obtained, the actual electron content $\bar{N}_{\mathrm{e}}^{(H)}$ can be determined using (5.3). Moreover, if there is a need to know the true range $R_{\boldsymbol{z}}$ of the chosen reference object, it can be easily found from either of the equations (5.4).

Let us emphasize that formula (5.5) does not degenerate in the sense that its denominator does not turn into zero. Indeed, if it were equal to zero, then system (5.4) would immediately yield $\omega_0 = \omega_1$. However, the quantity $\bar{\omega}_{\mathrm{pe}}^2$ computed according to (5.5) appears sensitive to the errors in the data $R_{\boldsymbol{y}}^{(0)}$ and $R_{\boldsymbol{y}}^{(1)}$. A rigorous analysis of this sensitivity, i.e., of the conditioning [37, Chap. 1] of formula (5.5), can be found in Appendix D. It shows that the conditioning is weakly affected only by how far the probing frequencies ω_0 and ω_1 are chosen from each other. For the most part, $\bar{\omega}_{\mathrm{pe}}^2$ appears sensitive to errors, because there is a difference between two large numbers that are close to one another ($R_{\boldsymbol{y}}^{(0)}$ and $R_{\boldsymbol{y}}^{(1)}$) in the numerator of (5.5). The overall conditioning of $\bar{\omega}_{\mathrm{pe}}^2$ can be improved, though, by using several reference locations instead of one. In Appendix D, we are showing that this approach indeed helps reduce the resulting error.

It is also to be noted that the idea of using two frequencies for determining the TEC is briefly mentioned in [44], without analyzing the resulting performance. The authors of [44] suggest, however, that the two frequencies be taken from the existing SAR bandwidth. This is likely to require that special strong scatterers (perhaps, artificial) be present in the imaged scene that can be used for deriving the ionosphere parameters from the raw SAR data. In the absence of such bright point targets the two frequencies have to be taken as two carriers so that the ionosphere parameters can be obtained from the processed SAR images.

6. Correcting the matched filter. Let us recall that the distortions of the SAR image are due to the mismatch between the actual field received by the radar antenna and the

assumptions made about this field when designing the signal processing algorithm, i.e., the matched filter. Once the quantity $\bar{N}_{\mathrm{e}}^{(H)}$ has been found, one can use formulae (3.25) and accurately evaluate the deterministic contributions to the travel times $T_{\mathrm{ph}}(\boldsymbol{x}^n, \boldsymbol{y}, \omega_0)$ and $T_{\mathrm{gr}}(\boldsymbol{x}^n, \boldsymbol{y}, \omega_0)$ for any location $\boldsymbol{y}$. Then one can also compute the pulse dilation for the reference point $\boldsymbol{y}$ using formula (3.27) and the new pulse rate according to (3.18). This allows one to correct the matched filter, i.e., to modify its definition in formulae (3.28) and (3.29) by substituting the travel times that account for the ionospheric dispersion.

6.1. Range resolution. The matched filter is corrected by using the actual travel times instead of the travel times in vacuum, and by taking into account the dilation and the rate change of the pulse upon its arrival. With this correction in place, the range factor of the generalized ambiguity function becomes (cf. formula (4.1))

(6.1)
$$W_R'(\boldsymbol{y},\boldsymbol{z}) = \int_{\max\{-\tau'(\boldsymbol{y})/2+2\tilde{T}_{\mathrm{gr}}(\boldsymbol{y}),\, -\tau'(\boldsymbol{z})/2+2T_{\mathrm{gr}}(\boldsymbol{z})\}}^{\min\{\tau'(\boldsymbol{y})/2+2\tilde{T}_{\mathrm{gr}}(\boldsymbol{y}),\, \tau'(\boldsymbol{z})/2+2T_{\mathrm{gr}}(\boldsymbol{z})\}} e^{-i\alpha'(\boldsymbol{y})(t-2\tilde{T}_{\mathrm{gr}}(\boldsymbol{y}))^2} e^{i\alpha'(\boldsymbol{z})(t-2T_{\mathrm{gr}}(\boldsymbol{z}))^2}\, dt$$
$$\propto \int_{\max\{-\tau'(\boldsymbol{y})/2+2\tilde{T}_{\mathrm{gr}}(\boldsymbol{y}),\, -\tau'(\boldsymbol{z})/2+2T_{\mathrm{gr}}(\boldsymbol{z})\}}^{\min\{\tau'(\boldsymbol{y})/2+2\tilde{T}_{\mathrm{gr}}(\boldsymbol{y}),\, \tau'(\boldsymbol{z})/2+2T_{\mathrm{gr}}(\boldsymbol{z})\}} e^{i(\alpha'(\boldsymbol{z})-\alpha'(\boldsymbol{y}))t^2} e^{4i(\alpha'(\boldsymbol{y})\tilde{T}_{\mathrm{gr}}(\boldsymbol{y})-\alpha'(\boldsymbol{z})T_{\mathrm{gr}}(\boldsymbol{z}))}\, dt,$$

where we have introduced the abbreviated notations $T_{\mathrm{gr}}(\boldsymbol{z}) = T_{\mathrm{gr}}(\boldsymbol{x}^0, \boldsymbol{z}, \omega_0)$ and $\tilde{T}_{\mathrm{gr}}(\boldsymbol{y}) = \tilde{T}_{\mathrm{gr}}(\boldsymbol{x}^0, \boldsymbol{y}, \omega_0)$. We emphasize that for the filter part of the generalized ambiguity function we can substitute only the deterministic component of the group travel time (5.2), because this is what we derive from the single-look information; see section 5. The primed quantities τ' and α' in formula (6.1) are to be evaluated for the pulse round trip between the antenna and the target (cf. formulae (3.17) and (3.18)):

$$\tau' = \tau + 2\delta\tau \quad \text{and} \quad \alpha' = \alpha - \delta\tau\frac{B}{\tau^2} = \frac{B}{2\tau}\left(1 - \frac{2\delta\tau}{\tau}\right), \tag{6.2}$$

where $\delta\tau$ is given by formula (3.27). For the integral (6.1), we consider the integration limits $\mp\tau'(\boldsymbol{y})/2 + 2\tilde{T}(\boldsymbol{y})$ and, changing the integration variable $u = t - 2\tilde{T}(\boldsymbol{y})$, obtain

$$W_R'(\boldsymbol{y},\boldsymbol{z}) \propto \int_{-\tau'(\boldsymbol{y})/2}^{\tau'(\boldsymbol{y})/2} e^{-i\alpha'(\boldsymbol{y})u^2} e^{i\alpha'(\boldsymbol{z})(u+2\tilde{T}_{\mathrm{gr}}(\boldsymbol{y})-2T_{\mathrm{gr}}(\boldsymbol{z}))^2}\, du$$
$$\propto \int_{-\tau'(\boldsymbol{y})/2}^{\tau'(\boldsymbol{y})/2} e^{i(\alpha'(\boldsymbol{z})-\alpha'(\boldsymbol{y}))u^2} e^{4i\alpha'(\boldsymbol{z})(\tilde{T}_{\mathrm{gr}}(\boldsymbol{y})-T_{\mathrm{gr}}(\boldsymbol{z}))u}\, du, \tag{6.3}$$

where the constant factors of magnitude one in front of the integrals are dropped.

Following the analysis of section 4.1, we first disregard the quadratic term $\sim u^2$ in the exponent under the integral (6.3), because this term is small. Then integral (6.3) evaluates to

$$W_R'(\boldsymbol{y},\boldsymbol{z}) \propto \tau'(\boldsymbol{y})\mathrm{sinc}[2\alpha'(\boldsymbol{z})(\tilde{T}_{\mathrm{gr}}(\boldsymbol{y}) - T_{\mathrm{gr}}(\boldsymbol{z}))\tau'(\boldsymbol{y})]. \tag{6.4}$$

The range resolution of the radar is defined as the full width of the sinc function (6.4) interpreted as a function of $R_{\boldsymbol{y}} - R_z$ and hence can be obtained by setting the argument of the sinc equal to 2π:

$$2\alpha'(\boldsymbol{z})(\tilde{T}_{\mathrm{gr}}(\boldsymbol{y}) - T_{\mathrm{gr}}(\boldsymbol{z}))\tau'(\boldsymbol{y}) = 2\pi.$$

With the help of (6.2), the previous equality transforms into

$$\frac{B}{\tau}\left(1-\frac{2\delta\tau}{\tau}\right)(\tilde{T}_{\mathrm{gr}}(\boldsymbol{y})-T_{\mathrm{gr}}(\boldsymbol{z}))\tau\left(1+\frac{2\delta\tau}{\tau}\right)=2\pi. \tag{6.5}$$

We first notice that the correction due to the dilation of the pulse in formula (6.5) becomes quadratic with respect to $\frac{2\delta\tau}{\tau}$. For the typical values of the parameters involved, we have $\frac{\delta\tau}{\tau}\sim 10^{-4}$; see [41]. Consequently, we can disregard this correction completely and instead of (6.5) write

$$B(\tilde{T}_{\mathrm{gr}}(\boldsymbol{y})-T_{\mathrm{gr}}(\boldsymbol{z}))=2\pi. \tag{6.6}$$

Then we can use formulae (3.25a), (4.6), (5.2), and (5.3) and express the difference between the group travel times in (6.6) as follows:

$$\tilde{T}_{\mathrm{gr}}(\boldsymbol{y})-T_{\mathrm{gr}}(\boldsymbol{z})=\frac{R_{\boldsymbol{y}}-R_{\boldsymbol{z}}}{c}\left(1+\frac{1}{2}\frac{\bar{\omega}_{\mathrm{pe}}^2}{\omega_0^2}\right)-\frac{1}{2}\frac{4\pi e^2}{m_{\mathrm{e}}\omega_0^2}\frac{1}{c}\varphi_0(\boldsymbol{z}). \tag{6.7}$$

As $\langle\varphi_0(\boldsymbol{z})\rangle=0$, we can say that for every particular realization of the random field μ we have $|\varphi_0(\boldsymbol{z}))|\sim\sqrt{\langle\varphi_0^2\rangle}$. Hence, the second term on the right-hand side of equality (6.7) appears much smaller than the first term, because the exact same argument applies here as given in section 4.1; see the discussion around (4.7). Thus, disregarding this second term and substituting the result into (6.6), we arrive at the following expression for the range resolution:

$$\Delta R=R_{\boldsymbol{y}}-R_{\boldsymbol{z}}\approx\frac{2\pi c}{B}\left(1-\frac{1}{2}\frac{\bar{\omega}_{\mathrm{pe}}^2}{\omega_0^2}\right). \tag{6.8}$$

The resolution given by formula (6.8) is an improvement over the noncorrected case (4.4), because it is basically as good as the nondispersive resolution $\Delta R=2\pi c/B$. However, as indicated in section 4.1, the range resolution of a SAR sensor does not suffer much from the ionospheric dispersion in any event. Therefore, what is even more important is that when the filter is corrected, the target is no longer shifted in range from its true position as in formula (4.3). That is because the maximum of the sinc in formula (6.4) is attained precisely at $R_{\boldsymbol{y}}=R_{\boldsymbol{z}}$.

What is also very important is that the degradation of image sharpness becomes negligible once the filter has been corrected. To analyze this effect, we bring back the quadratic term in the exponent under the integral (6.3). First, we recast this integral in the form

$$W_R'(\boldsymbol{y},\boldsymbol{z})\propto\int_{-\tau'(\boldsymbol{y})/2}^{\tau'(\boldsymbol{y})/2}e^{i\gamma u^2}e^{i\zeta u}du, \tag{6.9}$$

where

$$\gamma=\alpha'(\boldsymbol{z})-\alpha'(\boldsymbol{y})=\frac{B}{\tau^2}(\delta\tau(\boldsymbol{y})-\delta\tau(\boldsymbol{z}))=\frac{B}{\tau^2}\frac{2(R_{\boldsymbol{y}}-R_z)}{c}\frac{4\pi e^2}{m_{\mathrm{e}}\omega_0^2}\frac{B}{\omega_0}\mathcal{N}, \tag{6.10}$$

$$\zeta=4\alpha'(\boldsymbol{z})(\tilde{T}_{\mathrm{gr}}(\boldsymbol{y})-T_{\mathrm{gr}}(\boldsymbol{z})), \tag{6.11}$$

and the quantity $\mathcal{N}$ is defined in formula (3.26). The quadratic term in the exponent under the integral (6.9) is small: $|\gamma u^2| \ll 1$ for $u \in [-\tau'(\boldsymbol{y})/2, \tau'(\boldsymbol{y})/2]$, and consequently we have

$$W'_R(\boldsymbol{y},\boldsymbol{z}) \approx \int_{-\tau'(\boldsymbol{y})/2}^{\tau'(\boldsymbol{y})/2} (1+i\gamma u^2) e^{i\zeta u} du \tag{6.12}$$
$$= \tau' \mathrm{sinc}[2\alpha'(\boldsymbol{z})(\tilde{T}_{\mathrm{gr}}(\boldsymbol{y}) - T_{\mathrm{gr}}(\boldsymbol{z}))\tau'] + i\gamma \frac{4\zeta\tau' \cos\frac{\zeta\tau'}{2} + (-8+\zeta^2\tau'^2)\sin\frac{\zeta\tau'}{2}}{2\zeta^3},$$

where $\tau' = \tau'(\boldsymbol{y})$. The first term on the right-hand side of (6.12) obviously coincides with (6.4), and the second term represents a correction. According to (6.10) and (6.11), (6.7), both γ and ζ vanish as $R_{\boldsymbol{y}}$ approaches $R_{\boldsymbol{z}}$. However, the fraction on the right-hand side of (6.12) remains bounded as $\zeta \to 0$ (and $\gamma \to 0$). It is, in fact, easy to see that

$$W'_R(\boldsymbol{y},\boldsymbol{z}) \approx \tau' \mathrm{sinc}[2\alpha'(\boldsymbol{z})(\tilde{T}_{\mathrm{gr}}(\boldsymbol{y}) - T_{\mathrm{gr}}(\boldsymbol{z}))\tau'] + \frac{3}{16} i\gamma\tau'^3. \tag{6.13}$$

As the first term on the right-hand side of (6.13) is proportional to τ', the relative magnitude of the correction is $\sim \gamma\tau'^2$ (this is a dimensionless quantity). There is no correction at the central peak of the sinc, because $\gamma = 0$ when $R_{\boldsymbol{y}} = R_{\boldsymbol{z}}$. To quantify the extent to which the image sharpness is affected, we estimate the correction at the first zero of the sinc. Using formulae (6.10) and (6.2), we obtain

$$\gamma\tau'^2 = B\frac{2(R_{\boldsymbol{y}} - R_z)}{c}\frac{4\pi e^2}{m_{\mathrm{e}}\omega_0^2}\frac{B}{\omega_0}\mathcal{N}\left(1+\frac{2\delta\tau}{\tau}\right)^2,$$

where the value of $R_{\boldsymbol{y}} - R_{\boldsymbol{z}}$ shall be taken according to formula (6.8). For the typical values of the parameters involved, we have

$$\frac{4\pi e^2}{m_{\mathrm{e}}\omega_0^2}\mathcal{N} \approx \frac{\bar{\omega}_{\mathrm{pe}}^2}{\omega_0^2} \sim 10^{-4} \quad \text{and} \quad \frac{B}{\omega_0} \sim 10^{-2},$$

so that altogether we can write

$$\frac{3}{16}\gamma\tau'^2 \approx \frac{3\pi}{4}\frac{\bar{\omega}_{\mathrm{pe}}^2}{\omega_0^2}\frac{B}{\omega_0}\left(1-\frac{1}{2}\frac{\bar{\omega}_{\mathrm{pe}}^2}{\omega_0^2}\right)\left(1+\frac{4\delta\tau}{\tau}\right) \sim \frac{3\pi}{4}\cdot 10^{-6}.$$

We therefore conclude that the degradation of image contrast in range decreases to approximately 0.0002%, as opposed to 2% in the noncorrected case; see formula (4.5).

6.2. Azimuthal resolution. Once the matched filter has been corrected, expression (3.29) for the azimuthal component of the generalized ambiguity function becomes

$$W'_A(\boldsymbol{y},\boldsymbol{z}) = \sum_{n=-N/2}^{N/2} e^{2i\omega_0(\tilde{T}_{\mathrm{ph}}(\boldsymbol{x}^n,\boldsymbol{y},\omega_0) - T_{\mathrm{ph}}(\boldsymbol{x}^n,\boldsymbol{z},\omega_0))}, \tag{6.14}$$

where in the filter part we have substituted the deterministic portion of the phase travel time:

$$\tilde{T}_{\mathrm{ph}}(\boldsymbol{x}^0,\boldsymbol{z},\omega) = \frac{R_{\boldsymbol{z}}}{c}\left[1 - \frac{1}{\omega^2}\frac{4\pi e^2}{2m_{\mathrm{e}}}\frac{\bar{N}_{\mathrm{e}}^{(H)}}{H}\right],$$

because this is what we derive from the sing-look image by means of dual carrier probing; see section 5. Then, using formulae (3.25b), (4.8), and (4.9), we can transform expression (6.14) into (cf. formula (4.10))

$$W'_A(\boldsymbol{y},\boldsymbol{z}) \propto \sum_{n=-N/2}^{N/2} e^{\frac{2i\omega_0}{c}\left[-\frac{y_1 x_1^n}{R_0}\left(1-\frac{1}{2}\frac{4\pi e^2}{m_e\omega_0^2}\frac{\bar{N}_e^{(H)}}{H}\right)+\frac{1}{2}\frac{4\pi e^2}{m_e\omega_0^2}\varphi_n\right]}, \tag{6.15}$$

where the constant factor of unit magnitude in front of the sum was dropped. Next, following the same derivation as in section 4.2 (see also [41]), we compute the mean and variance of each term in the sum (6.15):

$$\begin{aligned}\left\langle e^{\frac{2i\omega_0}{c}\left[-\frac{y_1 x_1^n}{R_0}\left(1-\frac{1}{2}\frac{4\pi e^2}{m_e\omega_0^2}\frac{\bar{N}_e^{(H)}}{H}\right)+\frac{1}{2}\frac{4\pi e^2}{m_e\omega_0^2}\varphi_n\right]}\right\rangle \\ = e^{\frac{2i\omega_0}{c}\left[-\frac{y_1 x_1^n}{R_0}\left(1-\frac{1}{2}\frac{4\pi e^2}{m_e\omega_0^2}\frac{\bar{N}_e^{(H)}}{H}\right)\right]} e^{-\frac{1}{2}\frac{\omega_0^2}{c^2}\left(\frac{4\pi e^2}{m_e\omega_0^2}\right)^2\langle\varphi_n^2\rangle},\end{aligned} \tag{6.16}$$

$$\sigma_n^2 \approx \frac{\omega_0^2}{c^2}\left(\frac{4\pi e^2}{m_e\omega_0^2}\right)^2\langle\varphi_n^2\rangle. \tag{6.17}$$

Also as in section 4.2, the individual variances (6.17) can be assumed approximately equal to one another, $\sigma_n^2 \approx \sigma^2$, $n = -N/2,\dots,N/2$, because the integration distance for φ_n depends on n weakly. Hence, we can use (6.16) and derive the mean value of the sum (6.15):

$$\langle W'_A(\boldsymbol{y},\boldsymbol{z})\rangle \;\propto\; e^{-\sigma^2/2}\sum_{n=-N/2}^{N/2} e^{\frac{2i\omega_0}{c}\left[-\frac{y_1 x_1^n}{R_0}\left(1-\frac{1}{2}\frac{4\pi e^2}{m_e\omega_0^2}\frac{\bar{N}_e^{(H)}}{H}\right)\right]}. \tag{6.18}$$

The sum (6.18) can actually be computed using the same approach as employed in section 4.2 and in [41]. The result is another sinc function, and it leads to the following estimate of the azimuthal resolution in the case of a nonfluctuating ionosphere:

$$2y_1 \approx \frac{L}{2}\left(1+\frac{1}{2}\frac{4\pi e^2}{m_e\omega_0^2}\frac{\bar{N}_e^{(H)}}{H}\right) = \frac{L}{2}\left(1+\frac{1}{2}\frac{\bar{\omega}_{pe}^2}{\omega_0^2}\right).$$

This value is only marginally worse than that obtained in the nondispersive case: $2y_1 = L/2$. Even more important, correction of the filter restores the sharpness of the image for the nonfluctuating ionosphere, so that there is no deterioration like in the noncorrected case; see formula (4.15). The reason is that unlike in formula (4.10), there is no quadratic term with respect to x_1^n in the exponent in the sum (6.15).

As, however, the proposed correction is based on the single-look data that essentially do not account for randomness (due to the ergodicity), it does not offer any remedy for the stochastic part of image distortions in the azimuthal direction. In other words, we can expect that even with the corrected filter in place, the azimuthal factor $W'_A(\boldsymbol{y},\boldsymbol{z})$ of the generalized ambiguity function will still have the variance of order (4.16), which will result in the same extent of deterioration in the azimuthal resolution as estimated in [41].

7. Discussion. SAR images obtained from satellites are prone to deterioration due to the temporal dispersion of radio waves in the Earth's ionosphere. The deterioration is stronger for lower carrier frequencies and weaker for higher carrier frequencies. We have analyzed this phenomenon in the case of a scalar field (polarization of radar pulses is not taken into account) propagating in an inhomogeneous cold plasma. Our analysis shows that image deterioration is due to the mismatch between the actual signals scattered off the Earths' surface and received by the radar antenna and the matched filter (an image processing tool) designed as if the propagation between the antenna and the ground were unobstructed.

To correct the filter, one needs to know a key characteristic of the ionosphere precisely at the time and place the image is taken. This key characteristic is the integral content of electrons per unit area in the layer of ionospheric plasma between the satellite and the ground. We have proposed deriving this quantity by probing the terrain, and hence the ionosphere, on two distinct carrier frequencies. We have also shown that the resulting correction of the filter completely eliminates all the distortions of the image that are due to the deterministic part of the electron content in the ionosphere.

The correction, however, is not effective for removing the distortions due to the random part of the charged particle content, i.e., turbulent fluctuations of the electron number density. The reason is that the correction is based on the data from a single-look image, for which the effect of randomness is "downplayed" by ergodicity. Mitigating the stochastic part of image distortions will be a subject for future study.

Another issue that needs further attention is the sensitivity of the proposed dual carrier technique to the errors in the data. We have shown that this sensitivity can be reduced if multiple reference locations are used instead of a single one for evaluating the required electron content along the line of sight. It is possible that performing a statistical cross-correlation between the two images rather than considering individual reference locations may be even more efficient.

Besides, we should note that our approach to correcting the filter relies on the important consideration that the mean parameters of the ionosphere do not vary in the horizontal direction. This assumption will hold only if the size of the imaged scene is relatively small. For larger scenes, the procedure of dual carrier probing needs to be carried out repeatedly, and the filter needs to be adjusted accordingly, as the satellite travels along the orbit and the antenna's footprint sweeps the imaged stripmap.

Directions for the future study may include the following:

- An investigation of whether the stochastic component of image distortions can be tackled by any of the "black box" image sharpening and deblurring techniques developed previously in the general framework (see, e.g., [19]) with no direct relation to spaceborne SAR. The considerations based on the central limit theorem that are outlined in section 4.2 may be useful in this perspective.
- Introduction of a vector propagation model, analysis of SAR imaging with polarization, and accounting for anisotropy of the medium due to the magnetic field of the Earth and for the Faraday rotation.
- Analysis of the effect of turbulent fluctuations in the ionosphere on the image using true Kolmogorov-type spectra, as opposed to the modified spectrum (2.11), which accounts

only for the short range phenomena, and accounting for anisotropic turbulence due to the magnetic field of the Earth.
- Analysis of the cost and the engineering difficulties associated with the proposed dual carrier methodology. For example, how may the outcome be affected by the calibration differences between the electronic equipment used for the two carrier frequencies?
- Applying the proposed methodology to processing the actual experimental data.
- Approaches for reducing the noise that is always present, regardless of whether the imaging is done through the ionosphere or not, for example, instrument noise or rough terrain noise. As a minimum requirement, this noise may not be amplified by any of the techniques used for mitigating the ionospheric distortions.
- Analysis of the dispersion on the target, distinguishing between the target dispersion and the ionospheric dispersion, and possible applications to material identification SAR (MISAR).
- Optimization of interrogating waveforms for the ionosphere beyond the standard linear upchirps.

Appendix A. Propagation of radar pulses in the homogeneous ionosphere. We are interested in obtaining a spherically symmetric solution similar to the retarded potential (3.3), but for the case of dispersive propagation governed by the Klein–Gordon equation (2.6). Let $r = |\boldsymbol{z} - \boldsymbol{x}|$ denote the radial coordinate in the spherical system centered at $\boldsymbol{x} \in \mathbb{R}^3$, which is the location of the antenna (we are using the notation of section 3.1), and let $\varphi = \varphi(t, r)$ be a spherically symmetric solution of (2.6). Introduce a new function $\phi = \phi(t, r)$ such that $\varphi(t, r) = \phi(t, r)/r$; then $\phi(t, r)$ satisfies the one-dimensional Klein–Gordon equation

$$\frac{\partial^2 \phi}{\partial t^2} - c^2 \frac{\partial^2 \phi}{\partial r^2} + \omega_{\mathrm{pe}}^2 \phi = 0, \qquad r \geq 0. \tag{A.1}$$

Consequently, we need to look into the propagation of pulses governed by (A.1).

Assume that a pulse of shape $P(t)$ is given at $r = 0$ (location of the antenna); for example, it can be the high-range resolution upchirp (3.1):

$$P(t) = \frac{1}{4\pi} \chi_\tau(t) e^{i\left(\omega_0 + \frac{Bt}{2\tau}\right)t}, \tag{A.2}$$

where ω_0 is the center carrier frequency, B is the bandwidth, and τ is the duration of the chirp. The factor $1/4\pi$ in (A.2) accounts for the difference between the one-dimensional and three-dimensional delta-functions $\delta(r)$ and $\delta(x_1, x_2, x_3)$ that excite the pulse at the origin.

We will Fourier transform the pulse (A.2) in time and study the propagation of individual frequencies. The transformation yields

$$\begin{aligned} \hat{P}(\omega) &= \frac{1}{2\pi} \int_{-\tau/2}^{\tau/2} \frac{1}{4\pi} e^{i\left(\omega_0 + \frac{Bt}{2\tau}\right)t - i\omega t} dt = \frac{1}{8\pi^2} \int_{-\tau/2}^{\tau/2} e^{i\alpha t^2 + i\beta t} dt \\ &= \frac{1}{8\pi^2} \frac{\sqrt{\pi}}{2\sqrt{\alpha}} e^{-i\frac{\beta^2}{4\alpha} + i\frac{\pi}{4}} \left[\operatorname{erf}\left(\frac{\sqrt{-i}(\beta - \alpha\tau)}{2\sqrt{\alpha}} \right) - \operatorname{erf}\left(\frac{\sqrt{-i}(\beta + \alpha\tau)}{2\sqrt{\alpha}} \right) \right], \end{aligned} \tag{A.3}$$

where $\alpha = \frac{B}{2\tau}$ is the chirp rate, and $\beta = \omega_0 - \omega$. To simplify expression (A.3), we need to analyze the arguments of the erf functions. Denote

$$\eta_\pm = \frac{\beta \pm \alpha\tau}{2\sqrt{\alpha}} = \frac{\omega_0 - \omega \pm B/2}{\sqrt{2B/\tau}}, \tag{A.4}$$

and consider several cases. First, let $\omega \in [\omega_0 - B/2, \omega_0 + B/2]$, and in addition suppose that ω is not too close to either endpoint, $\omega_0 - B/2$ or $\omega_0 + B/2$. In other words, suppose that the numerator on the right-hand side of (A.4) is of the same order of magnitude as the bandwidth, i.e., $|\omega_0 - \omega \pm B/2| \sim B$. Then, $|\eta_\pm| \sim \sqrt{B\tau/2}$, and for the typical values of the parameters involved (see section 3) this quantity is approximately 15.8. In general, we can say that the value of $\sqrt{B\tau/2}$ is between 10 to 20 or higher, and we can therefore evaluate the erf functions on the right-hand side of (A.3) by the stationary phase method. Indeed,

$$\operatorname{erf}(\sqrt{-i}\eta_\pm) = \frac{2}{\sqrt{\pi}}\int_0^{\sqrt{-i}\eta_\pm} e^{-z^2}dz = \frac{2\sqrt{-i}}{\sqrt{\pi}}\eta_\pm\int_0^1 e^{i\eta_\pm^2 u^2}du = \frac{2\sqrt{-i}}{\sqrt{\pi}}\eta_\pm\left[\int_0^1 f_\delta(u)e^{i\eta_\pm^2 u^2}du + \mathcal{O}(\delta)\right],$$

where $f_\delta(u)$ is a specially chosen auxiliary function such that $f_\delta \in C^\infty[0,\,1]$, $f_\delta^{(k)}(1) = 0$ for all $k = 0, 1, 2, \ldots$, and $f_\delta(u) \equiv 1$ for $u \in [0, 1-\delta]$, where $\delta > 0$ can be arbitrarily small. Then, assuming that $\eta_\pm^2$ is sufficiently large, we can apply the Erdélyi lemma [13] to the last integral in the previous formula and by dropping the $\mathcal{O}(\delta)$ term obtain

$$\operatorname{erf}(\sqrt{-i}\eta_\pm) \approx \frac{2\sqrt{-i}}{\sqrt{\pi}}\eta_\pm\int_0^1 f_\delta(u)e^{i\eta_\pm^2 u^2}du \approx \frac{2\sqrt{-i}}{\sqrt{\pi}}\eta_\pm\frac{\Gamma(\frac{1}{2})}{2}e^{i\frac{\pi}{4}}\left(\eta_\pm^2\right)^{-1/2} = -\frac{\eta_\pm}{|\eta_\pm|}.$$

In doing so we note that in this particular case the asymptotic expansion given by the Erdélyi lemma actually converges, because all of its terms except for the leading term happen to be exactly equal to zero. Altogether, if ω is inside the interval $[\omega_0 - B/2, \omega_0 + B/2]$ and not too close to its endpoints, then we have

$$\hat{P}(\omega) \approx \frac{1}{8\pi^2}\frac{\sqrt{\pi}}{2\sqrt{\alpha}}e^{-i\frac{\beta^2}{4\alpha}+i\frac{\pi}{4}}\Bigg[\underbrace{-\frac{\eta_-}{|\eta_-|} + \frac{\eta_+}{|\eta_+|}}_{=2}\Bigg] = \frac{1}{8\pi^2}\frac{\sqrt{\pi}}{\sqrt{\alpha}}e^{-i\frac{\beta^2}{4\alpha}+i\frac{\pi}{4}}, \tag{A.5}$$

since in this case η_- is always negative, and η_+ is always positive.

Next, let ω be outside the interval $[\omega_0 - B/2, \omega_0 + B/2]$ and, again, not too close to either of its endpoints. Then we can apply the exact same reasoning as before and obtain

$$\hat{P}(\omega) \approx \frac{1}{8\pi^2}\frac{\sqrt{\pi}}{2\sqrt{\alpha}} e^{-i\frac{\beta^2}{4\alpha}+i\frac{\pi}{4}} \Bigg[\underbrace{-\frac{\eta_-}{|\eta_-|} + \frac{\eta_+}{|\eta_+|}}_{=0} \Bigg] = 0, \tag{A.6}$$

because unlike in formula (A.5), now both η_- and η_+ have the same sign.

Finally, we need to consider the case when ω is close to one of the endpoints of the interval $[\omega_0 - B/2, \omega_0 + B/2]$, i.e., $|\omega_0 - \omega - B/2| \ll B$ or $|\omega_0 - \omega + B/2| \ll B$. For example, if ω is close to the left endpoint so that $|\omega_0 - \omega - B/2|$ is small, then $\operatorname{erf}(\sqrt{-i}\eta_-)$ (see formulae (A.3) and (A.4)) can be evaluated using the first order Taylor expansion for erf, whereas $\operatorname{erf}(\sqrt{-i}\eta_+)$ should still be computed with the help of the Erdélyi lemma, which altogether yields

$$\hat{P}(\omega) = \frac{1}{8\pi^2}\frac{\sqrt{\pi}}{2\sqrt{\alpha}} e^{-i\frac{\beta^2}{4\alpha}+i\frac{\pi}{4}} \left[\frac{\sqrt{-i}}{\sqrt{\pi}\sqrt{\alpha}}(\omega_0 - \omega - B/2) + 1 \right]. \tag{A.7}$$

Expression (A.7) is valid only when the term in the round brackets is small.

Hereafter, we will leave out the foregoing transient case, $|\omega_0 - \omega - B/2| \ll B$ or $|\omega_0 - \omega + B/2| \ll B$, and evaluate the Fourier transform $\hat{P}(\omega)$ only by combining (A.5) and (A.6):

$$\hat{P}(\omega) \approx \begin{cases} \frac{1}{8\pi^2}\frac{\sqrt{\pi}}{\sqrt{\alpha}} e^{-i\frac{\beta^2}{4\alpha}+i\frac{\pi}{4}} & \text{if } \omega \in [\omega_0 - B/2, \omega_0 + B/2], \\ 0 & \text{if } \omega \notin [\omega_0 - B/2, \omega_0 + B/2]. \end{cases} \tag{A.8}$$

Qualitatively, formula (A.8) implies that in the spectrum of the pulse $P(t)$ (see (A.2)) we have only those frequencies ω that are built in there by design: $\omega_0 - B/2 \le \omega \le \omega_0 + B/2$. In reality, jump discontinuities that this pulse has at $\pm\tau/2$ will alter its spectrum to some degree, but we do not take this into account, because we disregard the transient behavior (A.7).

In the transformed space, each of the frequencies ω that compose the spectrum in (A.8), or, rather, each of the waves $e^{i\omega t}$, propagates with its own phase velocity. Indeed, the propagating pulse $\phi(t, r)$ that has covered the distance r from the origin can be written as the inverse Fourier transform [2, Chap. I], which immediately leads to the introduction of the phase velocity $v_{\mathrm{ph}} = v_{\mathrm{ph}}(\omega) = \omega/k$ in the exponent:

$$\phi(t, z) = \int_{\omega_0 - B/2}^{\omega_0 + B/2} \hat{P}(\omega) e^{i(\omega t - kr)} d\omega = \int_{\omega_0 - B/2}^{\omega_0 + B/2} \hat{P}(\omega) e^{i\omega(t - r/v_{\mathrm{ph}}(\omega))} d\omega. \tag{A.9}$$

The function $\hat{P}(\omega)$ in formula (A.9) is defined by (A.8), and the frequency ω and the wavenumber k are assumed to be connected via the dispersion relation (2.3). Next, recalling that the central carrier frequency is much higher than the Langmuir frequency, $\omega_0 \gg \omega_{\mathrm{pe}}$, and also that the radar pulse is narrow band, $|\omega - \omega_0| \ll \omega_0$, we can use formula (2.4) and obtain a

linearized expression for the phase velocity,

$$
\begin{aligned}
v_{\rm ph}(\omega) &= c\left(1+\frac{\omega_{\rm pe}^2}{c^2k^2}\right)^{1/2} = c\left(1+\frac{\omega_{\rm pe}^2}{\omega^2-\omega_{\rm pe}^2}\right)^{1/2} \approx c\left(1+\frac{1}{2}\frac{\omega_{\rm pe}^2}{\omega^2}\right)\\
&= c\left(1+\frac{1}{2}\frac{\omega_{\rm pe}^2}{\omega_0^2\left(1+\frac{\omega-\omega_0}{\omega_0}\right)^2}\right) \approx c\left(1+\frac{1}{2}\frac{\omega_{\rm pe}^2}{\omega_0^2}\left(1-2\frac{\omega-\omega_0}{\omega_0}\right)\right)\\
&= c\left(1+\frac{1}{2}\frac{\omega_{\rm pe}^2}{\omega_0^2}-\frac{\omega_{\rm pe}^2}{\omega_0^3}(\omega-\omega_0)\right),
\end{aligned}
\tag{A.10}
$$

as well as for its reciprocal, which is needed in (A.9):

$$
\frac{1}{v_{\rm ph}} \approx \frac{1}{c}\left(1-\frac{1}{2}\frac{\omega_{\rm pe}^2}{\omega_0^2}+\frac{\omega_{\rm pe}^2}{\omega_0^3}(\omega-\omega_0)\right).
$$

Then, substituting the reciprocal phase velocity into (A.9), we get

(A.11)

$$
\begin{aligned}
\phi(t,z) &\approx \frac{1}{8\pi^2}\frac{\sqrt{\pi}}{\sqrt{\alpha}}e^{i\frac{\pi}{4}}\int_{\omega_0-B/2}^{\omega_0+B/2} e^{-i\frac{\tau}{2B}(\omega-\omega_0)^2} e^{i\omega\left[t-\frac{r}{c}\left(1-\frac{1}{2}\frac{\omega_{\rm pe}^2}{\omega_0^2}+\frac{\omega_{\rm pe}^2}{\omega_0^3}(\omega-\omega_0)\right)\right]}d\omega\\
&= \frac{1}{8\pi^2}\frac{\sqrt{\pi}}{\sqrt{\alpha}}e^{i\frac{\pi}{4}}\int_{-B/2}^{B/2} e^{-i\frac{\tau}{2B}\lambda^2} e^{i(\omega_0+\lambda)\left[t-\frac{r}{c}\left(1-\frac{1}{2}\frac{\omega_{\rm pe}^2}{\omega_0^2}+\frac{\omega_{\rm pe}^2}{\omega_0^3}\lambda\right)\right]}d\lambda\\
&= \frac{1}{8\pi^2}\frac{\sqrt{\pi}}{\sqrt{\alpha}}e^{i\frac{\pi}{4}}e^{i\omega_0\left[t-\frac{r}{c}\left(1-\frac{1}{2}\frac{\omega_{\rm pe}^2}{\omega_0^2}\right)\right]}\int_{-B/2}^{B/2} e^{i\lambda\left[t-\frac{r}{c}\left(1-\frac{1}{2}\frac{\omega_{\rm pe}^2}{\omega_0^2}\right)-\frac{r}{c}\frac{\omega_{\rm pe}^2}{\omega_0^2}\right]} e^{i\lambda^2\left[-\frac{\tau}{2B}-\frac{r}{c}\frac{\omega_{\rm pe}^2}{\omega_0^3}\right]}d\lambda\\
&\approx \frac{1}{8\pi^2}\frac{\sqrt{\pi}}{\sqrt{\alpha}}e^{i\frac{\pi}{4}}e^{i\omega_0(t-r/v_{\rm ph}(\omega_0))}\int_{-B/2}^{B/2} e^{-ia\lambda^2+ib\lambda}d\lambda\\
&= \frac{1}{8\pi^2}\frac{\sqrt{\pi}}{\sqrt{\alpha}}e^{i\frac{\pi}{4}}\frac{\sqrt{\pi}}{2\sqrt{a}}e^{i\frac{b^2}{4a}}e^{-i\frac{\pi}{4}}e^{i\omega_0(t-r/v_{\rm ph}(\omega_0))}\left[\operatorname{erf}\left(\frac{\sqrt{i}(b-aB)}{2\sqrt{a}}\right)-\operatorname{erf}\left(\frac{\sqrt{i}(b+aB)}{2\sqrt{a}}\right)\right]\\
&= \frac{1}{16\pi\sqrt{\alpha}\sqrt{a}}e^{i\frac{b^2}{4a}}e^{i\omega_0(t-r/v_{\rm ph}(\omega_0))}\left[\operatorname{erf}\left(\frac{\sqrt{i}(b-aB)}{2\sqrt{a}}\right)-\operatorname{erf}\left(\frac{\sqrt{i}(b+aB)}{2\sqrt{a}}\right)\right],
\end{aligned}
$$

where $\lambda=\omega-\omega_0$, $a=\frac{\tau}{2B}+\frac{r}{c}\frac{\omega_{\rm pe}^2}{\omega_0^3}$, and $b=t-\frac{r}{c}(1+\frac{1}{2}\frac{\omega_{\rm pe}^2}{\omega_0^2})$.

Let us analyze the arguments of the erf functions in (A.11). First, we can write

$$
aB = \frac{\tau}{2}+\frac{r}{c}\frac{\omega_{\rm pe}^2}{\omega_0^2}\frac{B}{\omega_0} = \frac{\tau}{2}+\frac{\delta\tau}{2} \stackrel{\rm def}{=} \frac{\tau'}{2},
\tag{A.12}
$$

where $\delta\tau$ is the pulse dilation that it undergoes when traveling over the distance r, and τ', accordingly, is the new pulse length. Next, we can linearize the group velocity (2.5) the same

way as we have linearized the phase velocity (see (2.4) and (A.10)) and, using the first order Taylor formula, write

$$b \approx t - \frac{r}{c}\left(1 - \frac{1}{2}\frac{\omega_{\mathrm{pe}}^2}{\omega_0^2}\right)^{-1} \approx t - \frac{r}{v_{\mathrm{gr}}(\omega_0)}, \tag{A.13}$$

which means that b is the retarded moment of time that corresponds to the center carrier group velocity. Then, by applying the same stationary phase argument as we have used for the analysis of (A.3), we can conclude that if b of (A.13) is inside the interval $[-\tau'/2, \tau'/2]$ (see (A.12)), then the difference of the two erf functions on the last line of (A.11) is equal to 2, while otherwise this difference is equal to 0.

An important comment is in order. Leaving out the transients that correspond to the endpoints of the pulse and its spectrum is equivalent to disregarding the so-called precursors; see [17, sect. 21] or [35]. In other words, we are focusing on the propagation of the main body of the pulse, because it is the main body of the pulse that is used for building the generalized ambiguity function in section 3.

Finally, for the quantity $1/4a$ that is in the exponent on the last line of (A.11), we can write

$$\frac{1}{4a} = \frac{1}{\frac{2\tau}{B} + 4\frac{r}{c}\frac{\omega_{\mathrm{pe}}^2}{\omega_0^3}} = \frac{B}{2\tau + 4\frac{r}{c}\frac{\omega_{\mathrm{pe}}^2}{\omega_0^2}\frac{B}{\omega_0}} = \frac{B}{2\tau'} \stackrel{\mathrm{def}}{=} \alpha'. \tag{A.14}$$

Equation (A.14) introduces the new pulse rate α' (slope of the linear upchirp), which is smaller than the original pulse rate α. The relation between the two can be obtained as follows:

$$\alpha' = \frac{1}{\frac{2\tau}{B}\left(1 + 2\frac{r}{c}\frac{\omega_{\mathrm{pe}}^2}{\omega_0^3}\frac{B}{\tau}\right)} \approx \frac{B}{2\tau}\left(1 - 2\frac{r}{c}\frac{\omega_{\mathrm{pe}}^2}{\omega_0^3}\frac{B}{\tau}\right) = \alpha - \frac{r}{c}\frac{\omega_{\mathrm{pe}}^2}{\omega_0^3}\frac{B^2}{\tau^2} = \alpha - \frac{\delta\tau}{2}\frac{B}{\tau^2} \stackrel{\mathrm{def}}{=} \alpha + \delta\alpha. \tag{A.15}$$

When deriving (A.15), we could use the first order Taylor formula, because for the typical values of the parameters involved (see the end of section 2 and the beginning of section 3), the second term in the expression for a appears much smaller than the first term. Indeed, $\frac{\tau}{2B} \sim 2.5 \cdot 10^{-12}$, whereas for the propagation distances r about $1000km$ we have $\frac{r}{c}\frac{\omega_{\mathrm{pe}}^2}{\omega_0^3} \sim 3.3 \cdot 10^{-16}$.

We should also note that even though according to formulae (A.14), (A.15) there is a small difference between $1/4a$ and α, this difference can be disregarded when computing the first factor on the last line of (A.11), because taking it into account would imply only a minute change in the amplitude. Consequently,

$$\frac{1}{16\pi\sqrt{\alpha}\sqrt{a}} \approx \frac{1}{8\pi},$$

and, altogether, combining formulae (A.11)–(A.14) and recalling that $\varphi(t, r) = \phi(t, r)/r$, we obtain the spherically symmetric propagating pulse in the form

$$\begin{aligned}\varphi(t, r) &= \frac{1}{4\pi r} e^{i\omega_0(t - r/v_{\mathrm{ph}}(\omega_0))} \chi_{\tau'}(t - r/v_{\mathrm{gr}}(\omega_0)) e^{i\alpha'(t - r/v_{\mathrm{gr}}(\omega_0))^2} \\ &\stackrel{\mathrm{def}}{=} \frac{1}{4\pi r} A'(t - r/v_{\mathrm{gr}}(\omega_0)) e^{i\omega_0(t - r/v_{\mathrm{ph}}(\omega_0))}.\end{aligned} \tag{A.16}$$

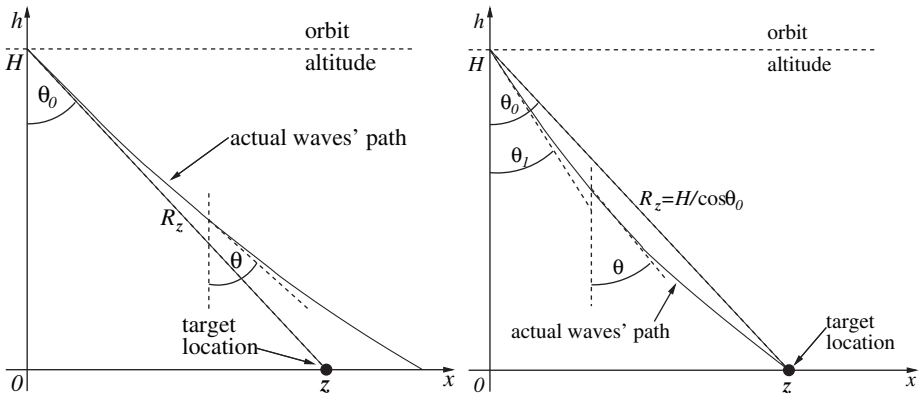

(a) With no correction of the look angle. (b) With the correction of the look angle.

Figure B.1. *Schematic waves' travel paths between the antenna and the target in the inhomogeneous ionosphere.*

Appendix B. Travel times in the deterministic inhomogeneous ionosphere. In this section, the quantities $N_e = N_e(h)$ and $\omega_{pe} = \omega_{pe}(h)$ are assumed to have no random component.

Suppose that the antenna is positioned at $x = 0$ and has altitude H above the Earth. It sends a signal toward the target z on the ground (see Figure B.1(a)) so that the look angle to the target is equal to θ_0 and, as such, $R_z = H/\cos\theta_0$. As the medium is lossless (collisionless dilute plasma with no Ohm conductivity; see section 2), its electric permittivity is real:

$$\epsilon(h) = 1 - \frac{\omega_{pe}^2(h)}{\omega^2}, \quad \text{where} \quad \omega_{pe}^2(h) = \frac{4\pi e^2 N_e(h)}{m_e}, \tag{B.1}$$

and we can write Snell's law (for plane waves) in the continuous form [17, sect. 19] as follows:

$$n(h)\sin\theta(h) = n(H)\sin\theta_0, \tag{B.2}$$

where the refraction index is given by

$$n(h) = \sqrt{\epsilon(h)} = \sqrt{1 - \frac{\omega_{pe}^2(h)}{\omega^2}}. \tag{B.3}$$

The angle $\theta(h)$ in formula (B.2) is the angle that the tangent to the wave trajectory at a given altitude h makes with the negative ordinate axis; see Figure B.1(a). Then, at every point on the trajectory, we can write with the help of (B.2)

$$\frac{dx}{dh} = -\tan\theta(h) = -\frac{n(h)\sin\theta(h)}{n(h)\cos\theta(h)} = -\frac{n(H)\sin\theta_0}{n(h)\cos\theta(h)} = -\frac{n(H)\sin\theta_0}{\sqrt{n^2(h) - n^2(H)\sin^2\theta_0}}. \tag{B.4}$$

Hence, the actual trajectory can be obtained by integrating equality (B.4):

$$x(h) = \int_H^h \frac{dx}{dh}dh = \int_h^H \frac{n(H)\sin\theta_0}{\sqrt{n^2(h) - n^2(H)\sin^2\theta_0}}dh. \tag{B.5}$$

However, for the general dependence $N_{\mathrm{e}} = N_{\mathrm{e}}(h)$, the integration in (B.5) is not easy to perform. On the other hand, we can simplify formula (B.4) by taking into account that all the ionospheric corrections are small and employing the first order Taylor expansion with respect to $\omega_{\mathrm{pe}}^2/\omega^2$:

$$\begin{aligned}\frac{dx}{dh} &= -\frac{\sqrt{1-\frac{\omega_{\mathrm{pe}}^2(H)}{\omega^2}}\sin\theta_0}{\sqrt{1-\frac{\omega_{\mathrm{pe}}^2(h)}{\omega^2}-\left(1-\frac{\omega_{\mathrm{pe}}^2(H)}{\omega^2}\right)\sin^2\theta_0}} \approx -\frac{\left(1-\frac{1}{2}\frac{\omega_{\mathrm{pe}}^2(H)}{\omega^2}\right)\sin\theta_0}{\sqrt{\cos^2\theta_0+\frac{\omega_{\mathrm{pe}}^2(H)\sin^2\theta_0-\omega_{\mathrm{pe}}^2(h)}{\omega^2}}} \\ &\approx -\tan\theta_0\left(1-\frac{1}{2}\frac{\omega_{\mathrm{pe}}^2(H)}{\omega^2}\right)\left(1-\frac{1}{2}\frac{\omega_{\mathrm{pe}}^2(H)\sin^2\theta_0-\omega_{\mathrm{pe}}^2(h)}{\omega^2\cos^2\theta_0}\right) \\ &\approx -\tan\theta_0\left(1-\frac{1}{2}\frac{\omega_{\mathrm{pe}}^2(H)-\omega_{\mathrm{pe}}^2(h)}{\omega^2\cos^2\theta_0}\right).\end{aligned} \tag{B.6}$$

The integration of equation (B.5) yields

$$\begin{aligned}x(h,\theta_0) &= \int_H^h -\tan\theta_0\left(1-\frac{1}{2}\frac{\omega_{\mathrm{pe}}^2(H)-\omega_{\mathrm{pe}}^2(h)}{\omega^2\cos^2\theta_0}\right)dh \\ &= (H-h)\tan\theta_0+\frac{1}{2}\frac{4\pi e^2}{m_{\mathrm{e}}}\frac{\tan\theta_0}{\omega^2\cos^2\theta_0}\left(\int_h^H N_{\mathrm{e}}(h)dh-(H-h)N_{\mathrm{e}}(H)\right).\end{aligned} \tag{B.7}$$

The shape of the curve (B.7) is determined by the profile of the electron number density $N_{\mathrm{e}} = N_{\mathrm{e}}(h)$. The curve is also parameterized by the look angle θ_0 at the location of the antenna. With no variation in the electron number density, $N_{\mathrm{e}}(h) \equiv N_{\mathrm{e}}(H)$, formula (B.7) yields a straight line between the antenna and the target:

$$x(h) = (H-h)\tan\theta_0. \tag{B.8}$$

As, however, $N_{\mathrm{e}}(h)$ is not constant, the ray that originates at the antenna under the look angle θ_0 will not, generally speaking, come to the target; see Figure B.1(a). To have this ray come to the target, we need to correct the look angle; see Figure B.1(b).

Let θ_1 be the new look angle. We substitute it into formula (B.7) instead of θ_0 and require that $x(0,\theta_1) = H\tan\theta_0$. In other words, we require that the wave trajectory that originates at the antenna under the new look angle θ_1 terminate precisely at the target $\boldsymbol{z}$ on the ground; see Figure B.1(b). We have[5]

$$x(0,\theta_1) = H\tan\theta_1+\frac{1}{2}\frac{4\pi e^2}{m_{\mathrm{e}}}\frac{\bar{N}_{\mathrm{e}}^{(H)}-N_{\mathrm{e}}(H)H}{\omega^2\cos^2\theta_1}\tan\theta_1 = H\tan\theta_0, \tag{B.9}$$

where $\bar{N}_{\mathrm{e}}^{(H)}$ is an important characteristic of the ionosphere—the integral of its electron number density across the layer of thickness H:

$$\bar{N}_{\mathrm{e}}^{(H)} \stackrel{\mathrm{def}}{=} \int_0^H N_{\mathrm{e}}(h)dh. \tag{B.10}$$

[5]Formula (B.9) corrects formula (D.2) from our previous publication on the subject [41, p. 177], in which we have committed an arithmetic error.

Formula (B.9) is an equation for θ_1. Let us now introduce a new notation K for brevity,

$$K = \frac{1}{2}\frac{4\pi e^2}{m_\mathrm{e}}\frac{\bar{N}_\mathrm{e}^{(H)} - N_\mathrm{e}(H)H}{\omega^2}, \tag{B.11}$$

and recast (B.9) as

$$H\tan\theta_1 + \frac{K}{\cos^2\theta_1}\tan\theta_1 = H\tan\theta_0. \tag{B.12}$$

Then, assuming that $\theta_1 = \theta_0 + \delta_\theta$, where $\delta\theta \ll \theta_0$, we can use the first order Taylor formula and write

$$\tan\theta_1 \approx \tan\theta_0 + \frac{\delta\theta}{\cos^2\theta_0} \quad \text{and} \quad \frac{1}{\cos^2\theta_1} \approx \frac{1}{\cos^2\theta_0}(1 + 2\tan\theta_0\delta\theta).$$

Substituting these expressions into (B.12), we arrive at

$$H\frac{\delta\theta}{\cos^2\theta_0} + \frac{K}{\cos^2\theta_0}(1 + 2\tan\theta_0\delta\theta)\left(\tan\theta_0 + \frac{\delta\theta}{\cos^2\theta_0}\right) = 0.$$

In the previous equation, we keep only linear terms with respect to $\delta\theta$:

$$H\delta\theta + K\tan\theta_0 + K\frac{2\sin^2\theta_0 + 1}{\cos^2\theta_0}\delta\theta = 0,$$

which yields

$$\delta\theta = -\frac{K\tan\theta_0}{H + K\frac{2\sin^2\theta_0+1}{\cos^2\theta_0}} = -\frac{K\tan\theta_0}{H}\frac{1}{1 + \frac{K}{H}\frac{2\sin^2\theta_0+1}{\cos^2\theta_0}} \approx -\frac{K\tan\theta_0}{H}\left(1 - \frac{K}{H}\frac{2\sin^2\theta_0+1}{\cos^2\theta_0}\right), \tag{B.13}$$

because according to formula (B.11), the quotient K/H is small: $K/H \sim \omega_\mathrm{pe}^2/\omega^2 \ll 1$. Our subsequent analysis shows that the second term in parentheses on the right-hand side of (B.13) can be disregarded.

Let s denote the arc length of the pulse trajectory. Then, using formula (B.4) and keeping only first order terms in the Taylor expansion, we can write

$$\frac{ds}{dh} = \sqrt{1 + \left(\frac{dx}{dh}\right)^2} = \sqrt{\frac{n^2(h)}{n^2(h) - n^2(H)\sin^2\theta_0}} \approx \frac{1}{\cos\theta_0}\left(1 + \frac{1}{2}\frac{\omega_\mathrm{pe}^2(h) - \omega_\mathrm{pe}^2(H)}{\omega^2}\tan^2\theta_0\right). \tag{B.14}$$

Consequently, the total length of the trajectory which originates at the angle θ_1 and is shown in Figure B.1(b) is given by

$$S = \int_0^H \frac{ds(\theta_1)}{dh}dh = \frac{1}{\cos\theta_1}\left(H + \frac{1}{2}\frac{4\pi e^2}{m_\mathrm{e}}\frac{\bar{N}_\mathrm{e}^{(H)} - \omega_\mathrm{pe}^2(H)H}{\omega^2}\tan^2\theta_1\right) = \frac{H}{\cos\theta_1}\left(1 + \frac{K}{H}\tan^2\theta_1\right). \tag{B.15}$$

For the trigonometric functions in formula (B.15), we can use (B.13) and write

$$\frac{1}{\cos\theta_1} \approx \frac{1}{\cos\theta_0}(1+\tan\theta_0\delta\theta) \approx \frac{1}{\cos\theta_0}\left[1-\frac{K\tan^2\theta_0}{H}\left(1-\frac{K}{H}\frac{2\sin^2\theta_0+1}{\cos^2\theta_0}\right)\right]$$
$$\approx \frac{1}{\cos\theta_0}\left[1-\frac{K\tan^2\theta_0}{H}\right]$$

and

$$\tan^2\theta_1 \approx \tan^2\theta_0 + \frac{2\tan\theta_0}{\cos^2\theta_0}\delta\theta \approx \tan^2\theta_0 - \frac{K}{H}\frac{2\tan^2\theta_0}{\cos^2\theta_0}\left(1-\frac{K}{H}\frac{2\sin^2\theta_0+1}{\cos^2\theta_0}\right)$$
$$\approx \tan^2\theta_0 - \frac{K}{H}\frac{2\tan^2\theta_0}{\cos^2\theta_0}.$$

On the right-hand side of the previous equalities, we have dropped the terms of order K^2/H^2, because $K/H \ll 1$, and hence the quantities quadratic with respect to K/H are negligible. We could have arrived at the same result if we had dropped the second term in parentheses on the right-hand side of the last equality in formula (B.13) ahead of time. Substituting the previous two expressions back into formula (B.15), we have

(B.16)
$$S = \frac{H}{\cos\theta_0}\left[1-\frac{K}{H}\tan^2\theta_0\right]\cdot\left[1+\frac{K}{H}\left(\tan^2\theta_0-\frac{K}{H}\frac{2\tan^2\theta_0}{\cos^2\theta_0}\right)\right] = \frac{H}{\cos\theta_0}\left[1+\mathcal{O}\left(\frac{K^2}{H^2}\right)\right].$$

Formula (B.16) implies that up to the negligibly small additive terms of order K^2/H^2, the length of the pulse trajectory between the antenna $\boldsymbol{x}$ and the target $\boldsymbol{z}$ (see Figure B.1(b)) is equal to the length of a straight line that connects the antenna and the target:

$$S \approx \frac{H}{\cos\theta_0} = |\boldsymbol{z}-\boldsymbol{x}| = R_{\boldsymbol{z}}. \tag{B.17}$$

The travel time along the trajectory (B.5) is given by the integral

$$T = \int_0^H \frac{dt}{dh}dh = \int_0^H \frac{1}{v(h)}\frac{ds}{dh}dh, \tag{B.18}$$

where $v(h) = v(\omega, \omega_{\mathrm{pe}}(h))$ can be either the group velocity (3.19) or the phase velocity (3.20), and the quantity $\frac{ds}{dh}$ is given by (B.14). For the case of group velocity, formula (B.18) yields

$$T_{\mathrm{gr}}(\boldsymbol{x},\boldsymbol{z},\omega) \approx \int_0^H \frac{1}{c}\left(1-\frac{1}{2}\frac{\omega_{\mathrm{pe}}^2(h)}{\omega^2}\right)^{-1}\frac{1}{\cos\theta_1}\left(1+\frac{1}{2}\frac{\omega_{\mathrm{pe}}^2(h)-\omega_{\mathrm{pe}}^2(H)}{\omega^2}\tan^2\theta_1\right)dh$$
$$\approx \frac{1}{c\cdot\cos\theta_1}\int_0^H\left(1+\frac{1}{2}\frac{\omega_{\mathrm{pe}}^2(h)}{\omega^2}+\frac{1}{2}\frac{\omega_{\mathrm{pe}}^2(h)-\omega_{\mathrm{pe}}^2(H)}{\omega^2}\tan^2\theta_1\right)dh, \tag{B.19}$$

because we are disregarding all the terms of higher order than linear with respect to $\omega_{\mathrm{pe}}^2/\omega^2$.

Formula (B.19), along with formulae (B.15) and (B.17), implies that

$$
\begin{aligned}
T_{\mathrm{gr}}(\boldsymbol{x},\boldsymbol{z},\omega) &\approx \frac{S}{c}+\frac{1}{c\cdot\cos\theta_1}\int_0^H \frac{1}{2}\frac{\omega_{\mathrm{pe}}^2(h)}{\omega^2}dh \\
&= \frac{H}{c\cdot\cos\theta_0}+\frac{1}{c\cdot\cos\theta_0}\left[1-\frac{K\tan^2\theta_0}{H}\right]\frac{1}{2}\frac{4\pi e^2}{m_{\mathrm{e}}}\frac{\bar{N}_{\mathrm{e}}^{(H)}}{\omega^2} \\
&\approx \frac{H}{c\cdot\cos\theta_0}\left(1+\frac{1}{2}\frac{4\pi e^2}{m_{\mathrm{e}}\omega^2}\frac{\bar{N}_{\mathrm{e}}^{(H)}}{H}\right)=\frac{R_{\boldsymbol{z}}}{c}\left(1+\frac{1}{2}\frac{4\pi e^2}{m_{\mathrm{e}}\omega^2}\frac{\bar{N}_{\mathrm{e}}^{(H)}}{H}\right),
\end{aligned}
\tag{B.20}
$$

where we have again dropped the terms higher than first order with respect to $K/H\sim\omega_{\mathrm{pe}}^2/\omega^2$. Formula (B.20) yields a final expression for the group travel time of a high frequency, $\omega\gg\omega_{\mathrm{pe}}$, radar pulse between the antenna and the target in an inhomogeneous deterministic ionosphere. Let us also recall that in our linearized framework the length of the pulse trajectory is equal to that of a straight segment between the antenna and the target, $S=R_{\boldsymbol{z}}$, because all the corrections are quadratic; see formulae (B.16) and (B.17). Hence, formula (B.20) could have been obtained merely as (cf. formula (B.18))

$$
\begin{aligned}
T_{\mathrm{gr}}(\boldsymbol{x},\boldsymbol{z},\omega) &= \int_0^{R_z}\frac{ds}{v_{\mathrm{gr}}(h)}=\frac{1}{\cos\theta_0}\int_0^H\frac{dh}{v_{\mathrm{gr}}(h)} \\
&\approx \frac{1}{c\cdot\cos\theta_0}\int_0^H\left(1+\frac{1}{2}\frac{\omega_{\mathrm{pe}}^2(h)}{\omega^2}\right)dh=\frac{R_{\boldsymbol{z}}}{c}\left(1+\frac{1}{2}\frac{4\pi e^2}{m_{\mathrm{e}}\omega^2}\frac{\bar{N}_{\mathrm{e}}^{(H)}}{H}\right).
\end{aligned}
\tag{B.21}
$$

Formula (B.21) can be interpreted in the context of the perturbation theory. Namely, the unperturbed pulse trajectory is a straight line. To get the first order perturbation for the group travel time, we integrate the reciprocal of the perturbed group velocity along the unperturbed trajectory.

As concerns the phase travel time, we need just to notice that the linearized group and phase velocities differ only by the sign of the $\sim\omega_{\mathrm{pe}}^2/\omega^2$ correction; see formulae (3.19) and (3.20). Hence, we have

$$
T_{\mathrm{ph}}(\boldsymbol{x},\boldsymbol{z},\omega)\approx\frac{R_{\boldsymbol{z}}}{c}\left(1-\frac{1}{2}\frac{4\pi e^2}{m_{\mathrm{e}}\omega^2}\frac{\bar{N}_{\mathrm{e}}^{(H)}}{H}\right).
\tag{B.22}
$$

Appendix C. Travel times in the stochastic ionosphere. The analysis of Appendix B indicates that we can use the geometrical optics perturbation method (see [39, Chap. I] for more detail) to derive the travel times of radar pulses in the turbulent ionosphere as well. In this case, the electron number density is a quasi-homogeneous random field (see formula (2.7)):

$$
N_{\mathrm{e}}=\langle N_{\mathrm{e}}(h)\rangle+\mu(\boldsymbol{x}),
\tag{C.1}
$$

and the dependence of μ on $\boldsymbol{x}$ in formula (C.1) means that μ depends on all spatial coordinates, $\boldsymbol{x}\in\mathbb{R}^3$.

Next, with no loss of generality, we can assume that the propagation plane (x, h) is fixed (see Figure B.1) and consider only two independent spatial variables. Moreover, recall that the random contribution to the electron number density is generally small compared to the deterministic part, because the quantity $M = \sqrt{\langle \mu^2 \rangle}/\langle N_{\rm e} \rangle$ introduced by formula (2.9) is small; see [1]. Consequently, we can still linearize with respect to the terms of order $\omega_{\rm pe}^2/\omega^2$ as done in Appendix B (high frequency regime) and write the equation for the pulse trajectory similar to (B.6) but with $\mu = \mu(x, h)$ taken into account:

$$\frac{dx}{dh} \approx -\tan\theta_0 \left(1 - \frac{1}{2}\frac{4\pi e^2}{m_{\rm e}} \frac{(\langle N_{\rm e}(H)\rangle - \langle N_{\rm e}(h)\rangle) + (\mu(0, H) - \mu(x, h))}{\omega^2 \cos^2\theta_0}\right). \tag{C.2}$$

Equation (C.2) is a first order ordinary differential equation that will be solved (approximately) by the perturbation method. First, we represent the solution in the form of a series:

$$x(h) = x^{(0)}(h) + x^{(1)}(h) + \cdots,$$

assuming that $x^{(0)} \sim 1$ and $x^{(1)} \sim \omega_{\rm pe}^2/\omega^2$, where $\omega_{\rm pe}^2/\omega^2$ is the small parameter for the asymptotic expansion.[6] Then, from (C.2), we immediately obtain the zeroth order contribution to the solution:

$$x^{(0)}(h) = \int_H^h -\tan\theta_0 dh = (H - h)\tan\theta_0, \tag{C.3}$$

which is a straight line between the antenna and the target; see Figure B.1 (also see formula (B.8)). For the first order correction, (C.2) yields

$$\frac{dx^{(1)}}{dh} = \tan\theta_0 \frac{1}{2}\frac{4\pi e^2}{m_{\rm e}} \frac{(\langle N_{\rm e}(H)\rangle - \langle N_{\rm e}(h)\rangle) + (\mu(0, H) - \mu(x^{(0)}(h), h))}{\omega^2 \cos^2\theta_0}. \tag{C.4}$$

Note that in order to write (C.4), we need an additional assumption that the derivative of μ with respect to x is no larger than order 1. Integrating (C.4) between H and h, we obtain

$$\begin{aligned} x^{(1)}(h) = \frac{1}{2}\frac{4\pi e^2}{m_{\rm e}} \frac{\tan\theta_0}{\omega^2 \cos^2\theta_0} \Bigg[&\left(\int_h^H \langle N_{\rm e}(h)\rangle dh - (H - h)\langle N_{\rm e}(H)\rangle \right) \\ &+ \left(\int_h^H \mu(x^{(0)}(h), h) dh - (H - h)\mu(0, H) \right) \Bigg]. \end{aligned} \tag{C.5}$$

If $\mu = 0$, then combining the zeroth order contribution (C.3) with the first order correction (C.5), we arrive at the previously obtained deterministic solution (B.7). Otherwise, for the solution $x(h) = x^{(0)}(h) + x^{(1)}(h)$ given by (C.3), (C.5) but with the adjusted look angle θ_1, we can write similarly to (B.9) and (B.12)

$$x(0, \theta_1) = H\tan\theta_1 + \frac{K}{\cos^2\theta_1}\tan\theta_1 = H\tan\theta_0, \tag{C.6}$$

[6] We do not formally introduce the second perturbation parameter, which would be of the order $\frac{4\pi e^2}{m_{\rm e}} \frac{\sqrt{\langle \mu^2 \rangle}}{\omega^2} \ll \frac{\omega_{\rm pe}^2}{\omega^2}$, because the quantity M of (2.9) is an altitude-independent constant, and hence the two parameters would be related to one another.

where the quantities K of (B.11) and $\bar{N}_{\rm e}^{(H)}$ of (B.10) are redefined as follows:

(C.7)
$$K = \frac{1}{2}\frac{4\pi e^2}{m_{\rm e}\omega^2}\left[\underbrace{(\bar{N}_{\rm e}^{(H)} - \langle N_{\rm e}(H)\rangle H)}_{\text{deterministic part}} + \underbrace{\left(\int_0^H \mu(x^{(0)}(h),h))dh - \mu(0,H)H\right)}_{\text{stochastic part}}\right] = \langle K\rangle + \eta$$

and

$$\bar{N}_{\rm e}^{(H)} \stackrel{\rm def}{=} \int_0^H \langle N_{\rm e}(h)\rangle dh. \tag{C.8}$$

Since $\sqrt{\langle\eta^2\rangle} < \langle K\rangle$ or even $\sqrt{\langle\eta^2\rangle} \ll \langle K\rangle$ (see the discussion right after (2.9)), and $\langle K\rangle/H \ll 1$, we can employ the same argument as in Appendix B and show using (C.6) that for any particular realization of μ the look angle increment $\delta\theta = \theta_1 - \theta_0$ will be given by the same expression (B.13) but with K and $N_{\rm e}^{(H)}$ defined by (C.7) and (C.8), respectively.

The arc length along the pulse trajectory with the look angle θ_1 can be found by integrating the differential equation (cf. formulae (B.14), (B.15))

$$\frac{ds}{dh} = \frac{1}{\cos\theta_1}\left(1 + \frac{1}{2}\frac{4\pi e^2}{m_{\rm e}}\frac{(\langle N_{\rm e}(H)\rangle - \langle N_{\rm e}(h)\rangle) + (\mu(0,H) - \mu(x,h))}{\omega^2}\tan^2\theta_1\right). \tag{C.9}$$

To integrate (C.9) we can again use the perturbation method. Representing $s(h)$ in the form

$$s(h) = s^{(0)}(h) + s^{(1)}(h) + \cdots,$$

we have the zeroth order term

$$s^{(0)}(h) = \frac{H-h}{\cos\theta_1} \tag{C.10}$$

and the first order term

$$\begin{aligned} s^{(1)}(h) = \frac{1}{2}\frac{4\pi e^2}{m_{\rm e}}\frac{\tan^2\theta_1}{\omega^2\cos\theta_1}\Bigg[&\left(\int_h^H \langle N_{\rm e}(h)\rangle dh - (H-h)\langle N_{\rm e}(H)\rangle\right) \\ &+ \left(\int_h^H \mu(x^{(0)}(h),h)dh - (H-h)\mu(0,H)\right)\Bigg]. \end{aligned} \tag{C.11}$$

To obtain the full length of the trajectory, we substitute $h = 0$ into formulae (C.10) and (C.11), and also use formula (C.7), which yields

$$S = s^{(0)}(0) + s^{(1)}(0) = \frac{H}{\cos\theta_1}\left(1 + \frac{K}{H}\tan^2\theta_1\right). \tag{C.12}$$

Expression (C.12) formally coincides with (B.15); only the definition of K is different. Consequently, we can repeat the argument from Appendix B and show that for every particular realization of μ the total length S of the pulse trajectory will be equal to that of a straight line

between the antenna and the target, up to the terms of order $\langle K\rangle^2/H^2$ that are negligible; see formulae (B.16) and (B.17):

$$S = \frac{H}{\cos\theta_0}\left[+\mathcal{O}\left(\frac{\langle K\rangle^2}{H^2}\right)\right] \approx \frac{H}{\cos\theta_0} = R_{\boldsymbol{z}}. \tag{C.13}$$

Finally, to obtain the group travel time, we need to integrate the following ordinary differential equation:

$$\begin{aligned}\frac{dt}{dh} &= \frac{1}{v_{\mathrm{gr}}(x,h)}\frac{ds}{dh} = \frac{1}{c}\left(1-\frac{1}{2}\frac{4\pi e^2}{m_{\mathrm{e}}}\frac{\langle N_{\mathrm{e}}(h)\rangle+\mu(x,h)}{\omega^2}\right)^{-1}\\ &\quad\cdot\frac{1}{\cos\theta_1}\left(1+\frac{1}{2}\frac{4\pi e^2}{m_{\mathrm{e}}}\frac{(\langle N_{\mathrm{e}}(H)\rangle-\langle N_{\mathrm{e}}(h)\rangle)+(\mu(0,H)-\mu(x,h))}{\omega^2}\tan^2\theta_1\right)\\ &\approx \frac{1}{c\cdot\cos\theta_1}\left(1+\frac{1}{2}\frac{4\pi e^2}{m_{\mathrm{e}}}\frac{\langle N_{\mathrm{e}}(h)\rangle+\mu(x,h)}{\omega^2}\right.\\ &\qquad\left.+\frac{1}{2}\frac{4\pi e^2}{m_{\mathrm{e}}}\frac{(\langle N_{\mathrm{e}}(H)\rangle-\langle N_{\mathrm{e}}(h)\rangle)+(\mu(0,H)-\mu(x,h))}{\omega^2}\tan^2\theta_1\right).\end{aligned} \tag{C.14}$$

As according to formula (C.13) the shape of the trajectory will not contribute to the travel time in the linearized framework, the integration of (C.14) by means of the perturbation method yields

$$\begin{aligned}T_{\mathrm{gr}}(\boldsymbol{x},\boldsymbol{z},\omega) &= \frac{H}{c\cdot\cos\theta_0}\left[1+\frac{1}{2}\frac{4\pi e^2}{m_{\mathrm{e}}\omega^2}\left(\frac{\bar{N}_{\mathrm{e}}^{(H)}}{H}+\frac{1}{H}\int_0^H\mu(x^{(0)}(h),h)dh\right)\right]\\ &= \frac{R_{\boldsymbol{z}}}{c}\left[1+\frac{1}{2}\frac{4\pi e^2}{m_{\mathrm{e}}\omega^2}\left(\frac{\bar{N}_{\mathrm{e}}^{(H)}}{H}+\frac{1}{R_{\boldsymbol{z}}}\int_0^{R_z}\mu(s)ds\right)\right].\end{aligned} \tag{C.15}$$

When deriving formula (C.15), we took into account that the look angle increment is small, $\delta\theta\sim\langle K\rangle/H$, as we did when deriving formula (B.20). We also note that the last integral in formula (C.15) shall be interpreted as taken along the unperturbed straight trajectory.

The phase travel time, as before, is obtained by changing the sign (cf. formula (B.22)):

$$T_{\mathrm{ph}}(\boldsymbol{x},\boldsymbol{z},\omega) = \frac{R_{\boldsymbol{z}}}{c}\left[1-\frac{1}{2}\frac{4\pi e^2}{m_{\mathrm{e}}\omega^2}\left(\frac{\bar{N}_{\mathrm{e}}^{(H)}}{H}+\frac{1}{R_{\boldsymbol{z}}}\int_0^{R_z}\mu(s)ds\right)\right]. \tag{C.16}$$

Appendix D. Conditioning of formula (5.5). If the quantity f depends on x, then the conditioning of $f(x)$, i.e., the sensitivity of f to the perturbations of x, is naturally defined as the maximum ratio of the relative error in f over the corresponding relative error in the input x; see [37, Chap. 1]:

$$\sup_{\delta x}\frac{|\delta f/f|}{|\delta x/x|} \approx |f'(x)|\frac{|x|}{|f|}.$$

In formula (5.5), the dependent quantity f is $\bar{\omega}_{\mathrm{pe}}^2$, and the input data are $R_{\boldsymbol{y}}^{(0)}$ and $R_{\boldsymbol{y}}^{(1)}$. Due to the obvious symmetry, it is sufficient to estimate the conditioning with respect to either of the two, and hereafter we will interpret $R_{\boldsymbol{y}}^{(0)}$ as the independent variable x. Then

$$\frac{\partial \bar{\omega}_{\mathrm{pe}}^2}{\partial R_{\boldsymbol{y}}^{(0)}} = \frac{2\omega_0^2\omega_1^2}{\omega_1^2 R_{\boldsymbol{y}}^{(1)} - \omega_0^2 R_{\boldsymbol{y}}^{(0)}} \left(1 + \frac{\omega_0^2 (R_{\boldsymbol{y}}^{(0)} - R_{\boldsymbol{y}}^{(1)})}{\omega_1^2 R_{\boldsymbol{y}}^{(1)} - \omega_0^2 R_{\boldsymbol{y}}^{(0)}}\right),$$

and hence the condition number of $\bar{\omega}_{\mathrm{pe}}^2$ with respect to $R_{\boldsymbol{y}}^{(0)}$ is given by

$$\begin{aligned} \left| \frac{\partial \bar{\omega}_{\mathrm{pe}}^2}{\partial R_{\boldsymbol{y}}^{(0)}} \frac{R_{\boldsymbol{y}}^{(0)}}{\bar{\omega}_{\mathrm{pe}}^2} \right| &= \left| \frac{R_{\boldsymbol{y}}^{(0)}}{R_{\boldsymbol{y}}^{(0)} - R_{\boldsymbol{y}}^{(1)}} + \frac{\omega_0^2 R_{\boldsymbol{y}}^{(0)}}{\omega_1^2 R_{\boldsymbol{y}}^{(1)} - \omega_0^2 R_{\boldsymbol{y}}^{(0)}} \right| \\ &\leqslant \frac{R_{\boldsymbol{y}}^{(0)}}{|R_{\boldsymbol{y}}^{(0)} - R_{\boldsymbol{y}}^{(1)}|} + \frac{\omega_0^2 R_{\boldsymbol{y}}^{(0)}}{|\omega_1^2 R_{\boldsymbol{y}}^{(1)} - \omega_0^2 R_{\boldsymbol{y}}^{(0)}|}. \end{aligned} \tag{D.1}$$

The first term on the right-hand side of (D.1) is large, because the ranges $R_{\boldsymbol{y}}^{(0)}$ and $R_{\boldsymbol{y}}^{(1)}$ are close to one another and the difference between the two is much smaller than each of them. The second term is not too large, because according to (5.4), the denominator $\omega_1^2 R_{\boldsymbol{y}}^{(1)} - \omega_0^2 R_{\boldsymbol{y}}^{(0)} = R_z(\omega_1^2 - \omega_0^2)$, and, consequently, the entire fraction is of the order $\omega_0^2/(\omega_1^2 - \omega_0^2)$, which is about 5 when the difference between ω_1 and ω_0 is 10%.

To improve the overall conditioning of $\bar{\omega}_{\mathrm{pe}}^2$, one can use several reference locations, $\boldsymbol{y}_1$, $\boldsymbol{y}_2$, $\boldsymbol{y}_3, \ldots$, instead of only one. Assume that we have computed $\bar{\omega}_{\mathrm{pe}}^2(\boldsymbol{y}_1)$, $\bar{\omega}_{\mathrm{pe}}^2(\boldsymbol{y}_2), \ldots, \bar{\omega}_{\mathrm{pe}}^2(\boldsymbol{y}_K)$ for K different reference locations according to formula (5.5) and that we evaluate $\bar{\omega}_{\mathrm{pe}}^2$ by plain averaging:

$$\bar{\omega}_{\mathrm{pe}}^2 = \frac{1}{K} \sum_{k=1}^{K} \bar{\omega}_{\mathrm{pe}}^2(\boldsymbol{y}_k). \tag{D.2}$$

Note that as $\bar{\omega}_{\mathrm{pe}}^2$ is a scalar quantity, formula (D.2) is equivalent to the least squares fit; see [37, Chap. 7].

Let us now interpret $\bar{\omega}_{\mathrm{pe}}^2(\boldsymbol{y}_k)$ as independent random variables with means $\langle \bar{\omega}_{\mathrm{pe}}^2(\boldsymbol{y}_k) \rangle$ and variances $\sigma^2(\bar{\omega}_{\mathrm{pe}}^2(\boldsymbol{y}_k))$, $k = 1, 2, \ldots, K$. Then (see, e.g., [11, Chap. 2])

$$\langle \bar{\omega}_{\mathrm{pe}}^2 \rangle = \frac{1}{K} \sum_{k=1}^{K} \langle \bar{\omega}_{\mathrm{pe}}^2(\boldsymbol{y}_k) \rangle \quad \text{and} \quad \sigma^2(\bar{\omega}_{\mathrm{pe}}^2) = \frac{1}{K^2} \sum_{k=1}^{K} \sigma^2(\bar{\omega}_{\mathrm{pe}}^2(\boldsymbol{y}_k)). \tag{D.3}$$

Assume, in addition and with no loss of generality, that the errors associated with computing the individual $\bar{\omega}_{\mathrm{pe}}^2(\boldsymbol{y}_k)$ are approximately equal to the corresponding standard deviations $\sigma(\bar{\omega}_{\mathrm{pe}}^2(\boldsymbol{y}_k))$ and that these errors are roughly the same for all $k = 1, 2, \ldots, K$. Then the second equality in formula (D.3) indicates that the overall error of evaluating $\bar{\omega}_{\mathrm{pe}}^2$ according to (D.2) will decrease proportionally to $K^{-1/2}$ as K increases.

Acknowledgments. The authors would like to thank Dr. Richard Albanese (AFRL), Prof. Margaret Cheney (RPI), Dr. Michael Gilman (NCSU), and Prof. Knut Solna (UC Irvine) for many useful discussions. We are also thankful to the two anonymous referees for their most helpful comments.

REFERENCES

[1] N. A. Armand, *Limitations to the resolution of satellite based synthetic aperture radars due to the conditions of the propagation of radio waves in the ionosphere*, Exploration of Earth from Space, (2005), pp. 27–38 (in Russian).
[2] M. Born and E. Wolf, *Principles of Optics: Electromagnetic Theory of Propagation, Interference and Diffraction of Light*, 7th (expanded) ed., Cambridge University Press, Cambridge, UK, 1999.
[3] B. C. Brock, *Ionospheric Effects on a Wide-Bandwidth, Polarimetric, Space-Based, Synthetic-Aperture Radar*, Technical report SAND-92-1967, UC-706, Sandia National Laboratory, Albuquerque, NM, 1993.
[4] W. D. Brown and D. C. Ghiglia, *Some methods for reducing propagation-induced phase errors in coherent imaging systems.* I. *Formalism*, J. Opt. Soc. Amer. A, 5 (1988), pp. 924–941.
[5] K. G. Budden, *The Propagation of Radio Waves: The Theory of Radio Waves of Low Power in the Ionosphere and Magnetosphere*, Cambridge University Press, Cambridge, UK, 1985.
[6] W. G. Carrara, R. S. Goodman, and R. M. Majewski, *Spotlight Synthetic Aperture Radar: Signal Processing Algorithms*, Artech House, Boston, 1995.
[7] M. Cheney, *A mathematical tutorial on synthetic aperture radar*, SIAM Rev., 43 (2001), pp. 301–312.
[8] M. Cheney and B. Borden, *Imaging moving targets from scattered waves*, Inverse Problems, 24 (2008), 035005.
[9] M. Cheney and B. Borden, *Fundamentals of Radar Imaging*, CBMS-NSF Regional Conf. Ser. in Appl. Math. 79, SIAM, Philadelphia, 2009.
[10] M. Cheney and C. J. Nolan, *Synthetic-aperture imaging through a dispersive layer*, Inverse Problems, 20 (2004), pp. 507–532.
[11] A. J. Chorin and O. H. Hald, *Stochastic Tools in Mathematics and Science*, Surv. Tutor. Appl. Math. Sci. 1, Springer, New York, 2006.
[12] P. H. Eichel and C. V. Jakowatz, Jr., *Phase-gradient algorithm as an optimal estimator of the phase derivative*, Optic Lett., 14 (1989), pp. 1101–1103.
[13] M. V. Fedoryuk, *The Saddle-Point Method [Metod perevala]*, Nauka, Moscow, 1977 (in Russian).
[14] G. Franceschetti and R. Lanari, *Synthetic Aperture Radar Processing*, Electronic Engineering Systems Series, CRC Press, Boca Raton, FL, 1999.
[15] W. B. Gail, *Effect of Faraday rotation on polarimetric SAR*, IEEE Trans. Aerospace Electron. Systems, 34 (1998), pp. 301–308.
[16] D. C. Ghiglia and W. D. Brown, *Some methods for reducing propagation-induced phase errors in coherent imaging systems.* II. *Numerical results*, J. Opt. Soc. Amer. A, 5 (1988), pp. 942–957.
[17] V. L. Ginzburg, *The Propagation of Electromagnetic Waves in Plasmas*, Int. Ser. Monogr. Electromagn.Waves 7, Pergamon Press, Oxford, UK, 1964.
[18] V. L. Ginzburg and A. V. Gurevich, *Nonlinear phenomena in a plasma located in an alternating electromagnetic field*, Soviet Phys. Uspekhi, 3 (1960), pp. 115–146.
[19] R. C. Gonzalez and R. E. Woods, *Digital Image Processing*, 3rd ed., Prentice–Hall, New York, 2008.
[20] A. L. Gray, K. E. Mattar, and G. Sofko, *Influence of ionospheric electron density fluctuations on satellite radar interferometry*, Geophys. Res. Lett., 27 (2000), pp. 1451–1454.
[21] A. V. Gurevich, *Nonlinear Phenomena in the Ionosphere*, Springer-Verlag, New York, 1978.
[22] A. V. Gurevich, *Nonlinear effects in the ionosphere*, Phys. Usp., 50 (2007), pp. 1091–1121.
[23] A. Ishimaru, Y. Kuga, J. Liu, Y. Kim, and T. Freeman, *Ionospheric effects on synthetic aperture radar at* $100MHz$ *to* $2GHz$, Radio Sci., 34 (1999), pp. 257–268.
[24] M. Jehle, M. Rüegg, L. Zuberbühler, D. Small, and E. Meier, *Measurement of ionospheric Faraday rotation in simulated and real spaceborne SAR data*, IEEE Trans. Geosci. Rem. Sens., 47 (2009), pp. 1512–1523.

[25] J.-S. Lee and E. Pottier, *Polarimetric Radar Imaging from Basics to Applications*, CRC Press, Boca Raton, FL, 2009.
[26] L. Li and F. Li, *Ionosphere tomography based on spaceborne SAR*, Adv. Space Res., 42 (2008), pp. 1187–1193.
[27] J. Liu, Y. Kuga, A. Ishimaru, X. Pi, and A. Freeman, *Ionospheric effects on SAR imaging: A numerical study*, IEEE Trans. Geosci. Rem. Sens., 41 (2003), pp. 939–947.
[28] K. E. Mattar and A. L. Gray, *Reducing ionospheric electron density errors in satellite radar interferometry applications*, Can. J. Rem. Sens., 28 (2002), pp. 593–600.
[29] D. B. Melrose and R. C. McPhedran, *Electromagnetic Processes in Dispersive Media: A Treatment Based on the Dielectric Tensor*, Cambridge University Press, Cambridge, UK, 1991.
[30] F. Meyer, R. Bamler, N. Jakowski, and T. Fritz, *The potential of low-frequency SAR systems for mapping ionospheric TEC distributions*, Geosci. Rem. Sens. Lett. IEEE, 3 (2006), pp. 2735–2744.
[31] A. S. Monin and A. M. Yaglom, *Statistical Fluid Mechanics: Mechanics of Turbulence. Volume* 1, The MIT Press, Cambridge, MA, 1971.
[32] A. S. Monin and A. M. Yaglom, *Statistical Fluid Mechanics: Mechanics of Turbulence. Volume* 2, The MIT Press, Cambridge, MA, 1975.
[33] P. M. Morse and H. Feshbach, *Methods of Theoretical Physics.* 2 *Volumes*, Int. Ser. Pure Appl. Phys., McGraw–Hill, New York, 1953.
[34] C. J. Nolan and M. Cheney, *Microlocal analysis of synthetic aperture radar imaging*, J. Fourier Anal. Appl., 10 (2004), pp. 133–148.
[35] K. E. Oughstun, *Electromagnetic and Optical Pulse Propagation* 1*: Spectral Representations in Temporally Dispersive Media*, Springer Ser. Opt. Sci. 125, Springer, New York, 2006.
[36] S. Quegan and J. Lamont, *Ionospheric and tropospheric effects on synthetic aperture radar performance*, Int. J. Rem. Sens., 7 (1986), pp. 525–539.
[37] V. S. Ryaben'kii and S. V. Tsynkov, *A Theoretical Introduction to Numerical Analysis*, Chapman & Hall/CRC, Boca Raton, FL, 2007.
[38] S. M. Rytov, Y. A. Kravtsov, and V. I. Tatarskii, *Principles of Statistical Radiophysics. Volume* 3*: Elements of Random Fields*, Springer-Verlag, Berlin, 1989.
[39] S. M. Rytov, Y. A. Kravtsov, and V. I. Tatarskii, *Principles of Statistical Radiophysics. Volume* 4*: Wave Propagation through Random Media*, Springer-Verlag, Berlin, 1989.
[40] V. I. Tatarskii, *Propagation of Waves in a Turbulent Medium*, Dover, New York, 1968.
[41] S. V. Tsynkov, *On SAR imaging through the Earth's ionosphere*, SIAM J. Imaging Sci., 2 (2009), pp. 140–182.
[42] S. V. Tsynkov, *On the use of start-stop approximation for spaceborne SAR imaging*, SIAM J. Imaging Sci., 2 (2009), pp. 646–669.
[43] D. E. Wahl, P. H. Eichel, D. C. Ghiglia, and C. V. Jakowatz, Jr., *Phase gradient autofocus—A robust tool for high resolution SAR phase correction*, IEEE Trans. Aerosp. Electron. Syst., 30 (1994), pp. 827–835.
[44] P. A. Wright, S. Quegan, N. S. Wheadon, and C. D. Hall, *Faraday rotation effects on L-band spaceborne SAR data*, IEEE Trans. Geosci. Rem. Sens., 41 (2003), pp. 2735–2744.
[45] Z.-W. Xu, J. Wu, and Z.-S. Wu, *A survey of ionospheric effects on space-based radar*, Waves Random Media, 14 (2004), pp. S189–S273.